

AD-A069 709

S H E CORP SAN DIEGO CA  
3 KHZ SQUID RECEIVER DEVELOPMENT.(U)

F/6 9/5

UNCLASSIFIED

MAY 78 M B SIMMONDS, W A FERTIG, R P GIFFARD  
SHE-77-60001

N00173-77-C-0210  
NL

| OF |  
AD  
A069 709

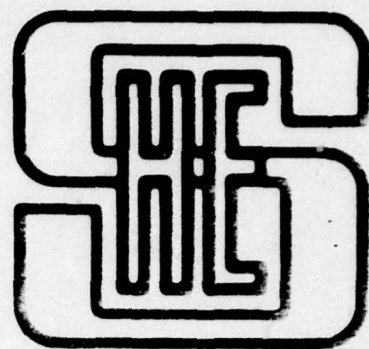


END  
DATE  
FILMED  
7-79  
DDC

18 NRL

19 542226

12



AD A 069709

LEVEL

9 Final rept. for 3 Aug 77-15 Apr 78  
on phase I,

Prepared for  
Naval Research Laboratory

by

10 M. B. Simmonds, W. A. Fertig ~~and~~ R. P. Giffard

SHE Report No. 77-60001

DDC  
RECEIVED  
JUN 11 1979  
C

11 May 1978

12 62 p.

APPROVED FOR PUBLIC RELEASE  
DISTRIBUTION UNLIMITED

14 SHE-77-60001

DDC FILE COPY

FINAL REPORT

6 3 kHz SQUID RECEIVER DEVELOPMENT.  
NRL # 542226  
PHASE I

CONTRACT NO. N00173-77-C-0210  
15

SHE CORPORATION  
CRYOGENIC INSTRUMENTS AND SYSTEMS  
4174 SORRENTO VALLEY BLVD.  
SAN DIEGO, CA 92121

TEL (714) 453-0300 TELEX 697903

79 05 30 249  
S/C 393 784

Sw

# FOREWARD

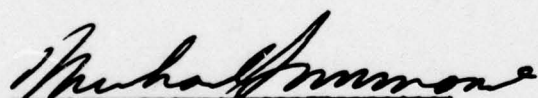
This report is submitted by S.H.E. Corporation in fulfillment of Contract No. N00173-77-C-0210 and covers all work done between 77 Aug 03 and 78 Apr 15.


This work was performed by the Research and Development department with consulting assistance from R.P. Giffard of Stanford University.

Dr. Giffard contributed to the initial design of the receiver and had primary responsibility for both the 60 MHz and 150 MHz SQUID amplifiers used in this work. W.A. Fertig performed much of the testing done on the Model Receiver, as well as assisting with the writing of this report. M.B. Simmonds had overall scientific responsibility for the work done under this contract.

Special acknowledgement is due J. Hancock and A. Knoll for typing, proofreading and assembling the manuscript.

Approved by

  
M.B. Simmonds  
Vice President, R & D

|   |  |
|---|--|
| Accession For   |  |
| NTIS GRA&I  | <input checked="checked" type="checkbox"/> |
| DDC TAB   | <input type="checkbox"/>                   |
| Unannounced   | <input type="checkbox"/>                   |
| Justification   |  |
| By _____  |  |
| Distribution/   |  |
| Availability Codes  |  |
| Dist  | Avail and/or special                       |
|  |  |

79 05 30 249



# ABSTRACT

We have designed and tested a model for a 3 kHz receiver using a superconducting antenna circuit and a SQUID (Superconducting QUantum Interference Device) amplifier. Q factors as high as 6400 have been demonstrated for the resonant antenna, giving it an extremely low intrinsic noise voltage. We have analyzed and solved various problems of matching between antenna and SQUID, as well as measuring noise contributed by materials in the surrounding cryostat. We have been able to use feedback from the SQUID amplifier into the antenna to effectively broaden the 3 dB bandwidth to 1200 Hz without raising the noise level of the system significantly. By scaling the results obtained with our model receiver to an antenna volume of .022 M<sup>3</sup> we have been able to estimate that a noise level of  $2.4 \times 10^{-17}$  T/ $\sqrt{\text{Hz}}$  could be obtained in a 100 Hz bandwidth.

M-cubed

(sq. rt. Hz)

$2.4 \times 10^{-17}$  to the -17th power

Key words: Antenna, Receiver, SQUID, Superconductivity, VLF Receiver.



## CONTENTS

|  | <u>PAGE</u> |
|--|-------------|
| 1 Introduction                                       |             |
| 1.1 Objectives and Scope of Project . . . . .        | 1           |
| 1.2 Organization of Report . . . . .                 | 3           |
| 2 Discussion of System Elements                      |             |
| 2.1 Induction Coil . . . . .                         | 5           |
| 2.2 Matching Transformer . . . . .                   | 9           |
| 2.3 Cryostat Dissipation . . . . .                   | 10          |
| 2.4 SQUID and SQUID Control Electronics . . . . .    | 11          |
| 2.5 Feedback Considerations . . . . .                | 12          |
| 3 Description of Components                          |             |
| 3.1 Dissipation Test Inductors . . . . .             | 13          |
| 3.2 Dissipation Test Capacitors . . . . .            | 13          |
| 3.3 Dissipation Test Probe . . . . .                 | 14          |
| 3.4 Cryostat Dissipation Test Fixtures . . . . .     | 14          |
| 3.5 Model Receiver Test Probe . . . . .              | 17          |
| 3.6 SQUID Electronics . . . . .                      | 21          |
| 3.7 Secondary Feedback . . . . .                     | 26          |
| 4 Description of Tests and Results                   |             |
| 4.1 Frequency Response of Model Receiver . . . . .   | 27          |
| 4.2 Gain of Model Receiver . . . . .                 | 30          |
| 4.3 Thermal Noise of Antenna . . . . .               | 31          |
| 4.4 Dissipation Due to Cryostat . . . . .            | 34          |
| 4.5 Noise of Model Receiver . . . . .                | 35          |
| 4.6 Dynamic Range of Model Receiver . . . . .        | 36          |
| 4.7 Linearity of Model Receiver . . . . .            | 38          |
| 5 Conclusions  |             |
| 5.1 Performance of a Full Scale Receiver . . . . .   | 42          |
| 5.2 Possibilities for Receiver Improvement . . . . . | 44          |

### TABLE

|  |    |
|--|----|
| 1.1 Target Specifications for the 3 kHz Receiver . . . . .     | 2  |
| 4.1 Receiver Voltage Gain Without Secondary Feedback . . . . . | 30 |
| 4.2 Resonant Circuit Characteristics . . . . .                 | 34 |
| 4.3 Interharmonic Distortion . . . . .                         | 41 |

### FIGURE

|  |    |
|--|----|
| 2.1 Model Receiver Block Program . . . . .                 | 6  |
| 3.1 Dissipation Test Probe . . . . .                       | 15 |
| 3.2 Mock-up of Full Scale Antenna Induction Coil . . . . . | 16 |

|   | <u>PAGE</u> |
|---|-------------|
| <u>FIGURE</u>   |             |
| 3.3 Model Receiver Probe — Mechanical Construction . . . . .  | 18          |
| 3.4 Model Receiver — Subsystem Schematic . . . . .            | 20          |
| 3.5 150 MHz SQUID Amplifier — Block Diagram . . . . .         | 22          |
| 3.6 VHF Amplifier Chain for 150 MHz SQUID Amplifier . . . . . | 23          |
| 3.7 Feedback Board for 150 MHz SQUID Amplifier . . . . .      | 25          |
| 4.1 Gain vs. Frequency for Model Receiver . . . . .           | 28          |
| 4.2 Phase vs. Frequency for Model Receiver . . . . .          | 29          |
| 4.3 Antenna Noise Test Setup . . . . .                        | 33          |
| 4.4 Noise vs. Frequency for Model Receiver . . . . .          | 37          |
| 4.5 Block Diagram of Linearity Test Setup . . . . .           | 39          |

|  |    |
|--|----|
| <u>APPENDIX</u>                                |    |
| A. Antenna Noise . . . . .                     | 46 |
| B. Antenna Energy Gain . . . . .               | 48 |
| C. Matching Transformer . . . . .              | 51 |
| D. Noise Contributions from Cryostat . . . . . | 53 |



## 1. INTRODUCTION

### 1.1 Objectives and Scope of Project

The spectrum of electromagnetic noise measured at the earth's surface exhibits a very sharp and deep local minimum at about 3 kHz. Most of the noise in this frequency region originates from worldwide thunderstorm activity. Atmospheric electric discharges generate strong VLF waves that propagate readily through the waveguide between the earth's surface and the ionosphere. A cutoff mode exists in this natural waveguide at about 3 kHz and gives rise to a strong, rather narrow attenuation band. Therefore, the background noise at 3 kHz is much less (perhaps 60 dB less<sup>1</sup>) than at other nearby frequencies.

The Navy is interested in communicating with receivers located beneath the ocean's surface. However, the relatively high conductivity of seawater (4 mho/m) gives rise to a rather strong attenuation, which is inversely proportional to the square root of the frequency. Thus, the lowest communication frequencies are receiving the greatest attention. Because the wavelength at these frequencies is very long it is difficult to provide compact antennas for either the transmitter or receiver. The requirement for a mobile underwater receiver demands that the size be very much less than a wavelength, and hence considerable attention is being given to improving the available sensitivity. The sharp noise minimum at 3 kHz makes this an attractive frequency for further study.

The free-space wavelength at 3 kHz is  $10^5$  m, and therefore only electrically small antennas can be considered. Recent measurements by NRL personnel indicate that the atmospheric noise level near 3 kHz is approximately -180 dBH. Since seawater attenuates 3 kHz signals at a rate of 1.8 dB/m, an atmospheric noise limited receiver must have a sensitivity of -216 dBH for operation at a depth of 20 m. An omnidirectional electric field antenna with this sensitivity lacks maneuverability because of its size. Although a trailing wire electric field antenna may be acceptable, it is not omnidirectional. However, it may be possible to supplement this with a properly oriented magnetic field induction coil to provide omnidirectionality or to use an H-field induction coil alone. An H-field sensitivity

---

<sup>1</sup>R. Barr, "The ELF and VLF Amplitude Spectrum of Atmospherics with Particular Reference to the Attenuation Band Near 3 kHz", J. Atmos and Terr. Physics, Vo. 32, pp, 977-990 (1970).



of  $2 \times 10^{-17} \text{ T}/\sqrt{\text{Hz}}$  is required if a 3 kHz receiver is to be atmospheric noise limited at a depth of 20 m. It was hoped that a SQUID-based receiver with a compact superconducting antenna could be made to have this very high level of magnetic field sensitivity over a useful communication bandwidth at this frequency.

The important target specifications that have been proposed by the Naval Research Laboratory for this receiver are listed in Table 1.1.

Table 1.1  
Target Specifications for the 3 kHz Receiver

|                          |   |
|--------------------------|---|
| Antenna Orientation      | Sensitive to horizontal magnetic field.   |
| Receiver Noise           | $2 \times 10^{-17} \text{ T rms}/\sqrt{\text{Hz}}$ , referred to input, within passband.  |
| Center Frequency         | $(3 \pm 0.01) \text{ kHz}$ .  |
| Bandwidth                | -3 dB points at $\pm 100 \text{ Hz}$ from center frequency.   |
| Dynamic Range            | 130 dB at center frequency referred to rms noise in unit bandwidth.   |
| Linearity                | $\pm 2 \times 10^{-16} \text{ T rms}$ . In-band IM products from mixing out-of-band (OOB) signals not to exceed $2 \times 10^{-17} \text{ T rms}/\sqrt{\text{Hz}}$ for OOB signal amplitudes equal to $5 \times 10^{-8} \text{ T}$ or the maximum amplitude that can be received at the OOB frequency without flux jumping (or other nonlinearity), whichever is smaller. |
| Gain Stability           | Closed-loop gain (magnitude and phase) stable $1/10^4$ for conditions given in environmental specification.   |
| Dewar Transparency       | 0.5 dB maximum attenuation at 3 kHz during normal operation.  |
| Reduced Sensitivity Mode | Reversible means to give a precisely known, 10-fold reduction in sensitivity stable to 0.1% on thermal cycling.   |
| Calibration Coil         | To verify operational capability and approximate gain calibration; mounted within cryostat.   |
| Output                   | Linear, analog output spanning $\pm 10 \text{ V}$ without reset.  |

#### System Configuration

Control chassis with all adjustments and outputs required for normal field operation to be separable from antenna dewar and input amplifier by at least 200 m without degrading other specifications.

#### Environmental

All specifications to be met for ambient temperature and humidity between 0 - 40°C and 0 - 80%, respectively, for all levels of receivable input signals.

#### Operating Time

7 days between helium refills.

#### Dewar Vacuum

To be maintained without pumping when dewar is at 77 K or below. Re-evacuation with mechanical pump only shall be sufficient.

#### Dimensions

The dewar together with all receiver components that must be located nearby shall fit into a cylinder 33.6 cm ID x 153 cm long.

#### Power Requirements

110 V, 60 Hz, single phase. Provision for battery operation.

Meeting these specifications will require a significant advance in the state-of-the-art for SQUID-based magnetometers. The target field sensitivity alone represents a 500-fold improvement in performance. Therefore, several preliminary studies are needed before a full scale prototype receiver can be properly designed. First, we must determine how to build an enclosure for the superconducting elements which does not introduce magnetic noise into the receiver. Second, we must find appropriate materials and construction techniques for the induction coil circuit in order to obtain the required intrinsic antenna noise level. Third, we must learn how to properly couple the induction loop to the SQUID. Finally, we must optimize the feedback configuration to achieve the target bandwidth.

The goal of the work presented in this report is to improve our understanding of these important problem areas. Once they have been carefully investigated, we can construct a model receiver, measure its characteristics, and extrapolate them to predict the performance of a full scale system.

#### 1.2 Organization of Report

Section 2 discusses the various elements of the receiver in general terms and, with the aid of appendices, develops the equations necessary for a quantitative analysis of the system. Section 3 describes the physical and electrical characteristics of the components and fixtures which have been constructed in

connection with this project. Section 4 presents both the test procedures used and the results obtained to establish how closely the target specifications have been achieved. Section 5 concludes with some comments about the extrapolation of the performance of our model system to a full scale receiver and also identifies areas where further measurements or development work would be important.



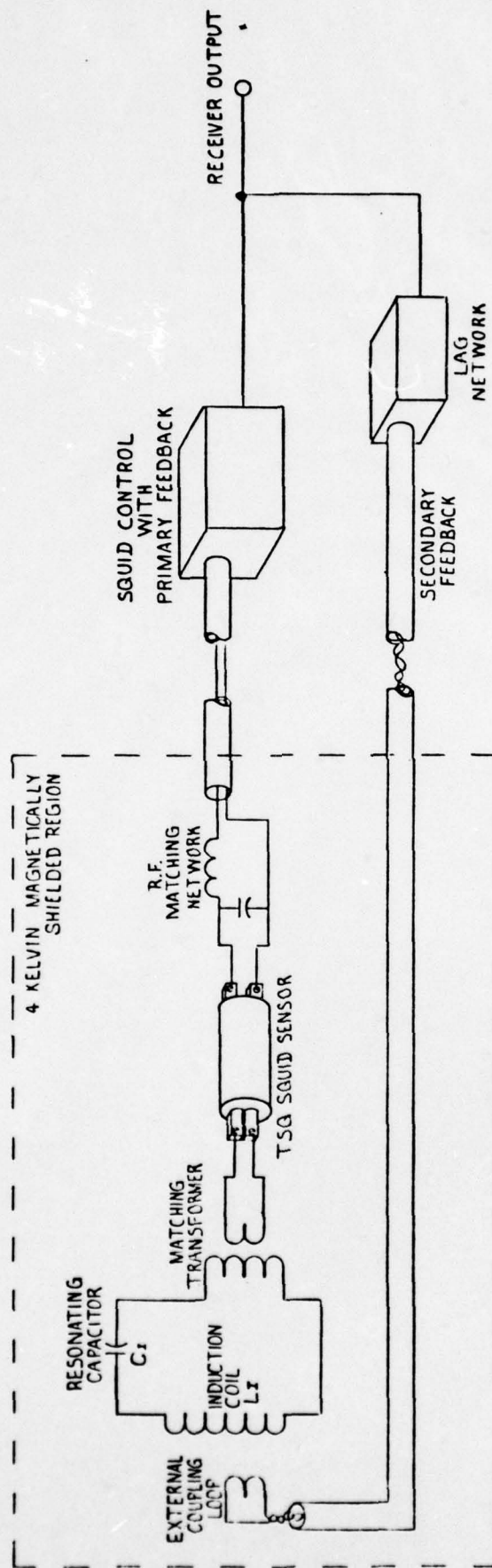
## 2. DISCUSSION OF SYSTEM ELEMENTS

### 2.1 Induction Coil

An induction coil is used to couple the receiver to the external magnetic field. The receiver's sensitivity is proportional to the total sampled volume of external field, so the coil's volume should be as large as specifications permit to achieve maximum performance. Unfortunately the inductance of such a receiving coil is significantly greater than the inductance of any reasonable SQUID input coil. A straightforward solution to this problem is to use a matching transformer between the induction coil and the SQUID. This input circuit configuration is shown in Fig. 2.1. The theoretical improvement obtained from this transformer is described in Section 2.2. The values of the components and the details of their construction will be discussed in Section 3.5.

Since we are only interested in receiving signals relatively near 3 kHz, we have chosen to resonate the induction coil with a capacitor at this center frequency. The advantages are two-fold. First, the resulting increase in the coil's current gain in the bandwidth of interest reduces the sensitivity requirements placed on the SQUID. Second, the resonating capacitor rolls off the receiver's sensitivity to slowly varying fields. This last effect is critically important for an instrument of this sensitivity. If the receiver retained its target sensitivity of  $2 \times 10^{-17} \text{ T}/\sqrt{\text{Hz}}$  down to low frequencies, then rotational motion of only  $2 \times 10^{-6}$  radians would give a full scale response and cause severe problems with dynamic range.

A basic requirement placed on this input circuit is that its intrinsic thermal noise voltage per unit bandwidth must be less than the E.M.F. induced by a 3 kHz,  $2 \times 10^{-17} \text{ T}/\sqrt{\text{Hz}}$  magnetic field. The effective series resistance in the resonant circuit behaves like a 4.2 K white noise source. Since it also determines the quality factor  $Q$  of the circuit, this effective resistance may easily be determined by measuring the sharpness of the resonance. In Appendix A we develop an expression for the field noise level  $B_n$  of our input circuit in terms of its temperature, dimensions, resonant frequency, and  $Q$  factor. The result is that



MODEL RECEIVER BLOCK DIAGRAM  
FIG 2.1

$$B_n / \sqrt{\text{Hz}} = \left( \frac{4\mu_0 \lambda k_B T_F}{\omega_0 Q A \ell} \right)^{1/2} \quad (2.1.1)$$

Here,  $\lambda$  is a calculable shape factor or order unity<sup>2</sup>,  $T_F$  is the circuit temperature, and  $A$  and  $\ell$  are the area and length of the loop, respectively.

Given the size limitations placed on the receiver package (33.6 cm diameter  $\times$  152 cm height) we estimate that our helium chamber can have a maximum diameter of 24 cm and a maximum height of about 76 cm. If we use a rectangular cross section induction loop which fills the cryostat we are thus limited to a coil 76 cm high  $\times$  17 cm wide  $\times$  17 cm long. This coil has a volume of  $2.2 \times 10^4 \text{ cm}^3$  and  $\lambda$  is 0.56. Using these values in Eq. 2.1.1 we find that for an intrinsic noise level of  $10^{-17} \text{ T}/\sqrt{\text{Hz}}$  we would need a  $Q$  of at least  $10^3$  in our circuit.

It should be pointed out that the requirement of a high  $Q$  in the preceding discussion does not in itself imply any basic restriction on the receiver's bandwidth. With a sufficiently quiet following amplifier the 3 dB bandwidth can be arbitrarily broadened through feedback. The  $Q$  factor in this context is important only in determining the intrinsic magnetic field noise of the coil.

Dissipation in this resonant circuit can come from ac resistance in the coil, the capacitor, or the transformer. Since these sources of loss are all at the same temperature (4.2 K) they affect the  $Q$  factor and the noise level identically and need not be determined separately. We believe that the primary cause of dissipation in this circuit is hysteretic flux motion in the superconducting materials used in the induction loop, the transformer, and the capacitor plates. It is possible that there is also some contribution from hysteresis in the capacitor dielectric, although we have no way to estimate its relative magnitude.

It would be difficult to directly test the  $Q$  of an induction coil having the size and geometry needed for the actual receiver. Its strong coupling to the surrounding space would require the design and construction of a large, electromagnetically transparent cryostat. Although we have, as part of this project, determined how to design such a cryostat we did not propose to actually construct it. We have therefore tested the  $Q$  factor for large superconducting coils by winding them

<sup>2</sup>F.W. Grover, Inductance Calculations Working Formulas and Tables. New York: Dover, pp. 170 - 176 (1970)



in a toroidal geometry. This type of coil can be enclosed in a loosely fitting superconducting shield to which it does not couple very strongly. The construction of the cryostat is thus unimportant and we have used one that was available at our facility. The details of this test and the equipment used in it are described elsewhere.

Another possible contributor to noise voltage in the resonant input circuit is the SQUID itself. This noise is coupled back through the matching transformer and added to the other voltages. It is not the same noise which is generally referred to in defining SQUID performance. The conventional noise is a current (or flux) noise which is used to define the energy sensitivity or "flux quantum resolution" of the SQUID. The voltage noise was predicted by Enholm as a general property of rf-biased SQUIDS, and is due to a reverse transfer of power from the SQUID output. It is extremely small and usually unobservable in conventional input circuits. However, the high Q input circuit used in this receiver may make this new noise source noticeable in a very narrow bandwidth around the resonant frequency.

Another basic specification for the induction coil antenna is its energy gain. In Appendix B we derive an equation for the energy available to the SQUID for a given applied field  $B_0$ :

$$\frac{E_c}{B_0^2} = \left( \frac{A\ell}{2\mu_0\lambda} \right) \left( \frac{\omega_0}{2\Delta\omega} \right)^2 \frac{\gamma}{(1 + \gamma)^2} . \quad (2.1.2)$$

Here  $\Delta\omega$  is the circuit bandwidth and  $\gamma$  is the ratio between the effective inductance of the following amplifier and that of the induction coil. Note that our expression for gain has assumed the "worse case" situation at the band limits where  $\omega = \omega_0 \pm \Delta\omega$ .

As  $\omega$  approaches  $\omega_0$ , Eq. B.3 shows that the power gain increases quadratically until it finally becomes limited by the Q of the resonant circuit. For the high Q circuit under consideration here this limitation is not reached until the frequency is within about 1 Hz of resonance. The important point is that if the SQUID amplifier is the limiting factor in the receiver's noise level, then reducing the

<sup>3</sup>Enholm, G., J. Low Temp. Phys. 29, 1 (1977)

required bandwidth will proportionately reduce the spectral density of the magnetic field noise. However, for bandwidths less than  $\omega_0/Q$ , no further improvement can be obtained since the antenna's power gain is then limited by its  $Q$ .

## 2.2 Matching Transformer

The location of this component is shown in Fig. 2.1. It serves to "transform up" the inductance which the SQUID presents to the resonant circuit. This transformed inductance is the  $L_C$  described in Appendix B. An important result obtained in this appendix is contained in Eq. B.10 which allows us to quantitatively analyze the energy loss due to mis-matching between the induction coil and the effective coupling inductor. The fraction of induction coil energy actually reaching the SQUID is given by the factor  $\gamma/(1 + \gamma)^2$  where  $\gamma \equiv L_C/L_I$ . Here,  $L_C$  is the transformed SQUID inductance and  $L_I$  is the induction coil inductance.

In the absence of any transformer, the SQUID presents its actual input coil inductance to the resonant circuit. Its value is typically 2  $\mu$ H for toroidal rf SQUIDs. The induction coil, on the otherhand, must be of the order of 25 mH if it is to be resonated at 3 kHz with a reasonable size superconduction capacitor. Thus, with no transformer the energy made available to the SQUID is reduced by a factor of  $10^4$  from the theoretical maximum.

If the transformer were ideal, the SQUID's apparent inductance could be transformed up as the turns ratio squared while its current gain was increased linearly. Thus, this transformer would not degrade the SQUID energy sensitivity. The detailed analysis of the non-ideal transformer is presented in Appendix C. One of the important results of this analysis is that, given the transformer coupling coefficient  $K$ , we can write the energy efficiency  $\alpha$  as

$$\alpha = \frac{K^2}{[1 + (1-K^2)^{1/2}]^2} \quad (2.2.1)$$

By combining Eq. B.8 and Eq. C.13 we may write an overall expression for current sensitivity taking into account both impedance mis-matching and transformer losses.

The result is

$$\frac{I_{\text{SQUID}}}{B_{\text{ANTENNA}}} = \left( \frac{L_I}{L_S} \right)^{\frac{1}{2}} \left( \frac{\gamma^{\frac{1}{2}}}{(1 + \gamma)} \right) \left( \frac{\omega N A}{2 \Delta \omega L_I} \right) \alpha^{\frac{1}{2}} \quad (2.2.2)$$

In this equation  $N$  is the number of turns on the inductance coil and  $L_S$  in the SQUID inductance. This is a useful form because the significance of the factors is readily apparent. Factor one is a basic inductance ratio, factor two describes the degree of matching to the induction loop, factor three gives the physical and electrical characteristics of the induction loop, and factor four gives the loss due to a non-ideal transformer.

The above equation may be cast into a different form where the factors have an even greater physical significance. We may eliminate  $L_I$  by use of Eq. B.7, and obtain an expression for energy delivered to the SQUID,  $E_{\text{SQUID}} \equiv \frac{1}{2} L_S I_S^2$

$$\frac{E_{\text{SQUID}}}{B^2_{\text{ANTENNA}}} = \frac{\alpha}{2} \left( \frac{\gamma}{(1 + \gamma)^2} \right) \left( \frac{\omega}{2 \Delta \omega} \right) \left( \frac{v}{\mu_0 \lambda} \right) \quad (2.2.3)$$

where we define the physical volume of the antenna  $v \equiv A \lambda$ .

This form is the most general because it removes all reference to any particular choices of impedance and shows the essential characteristic of the induction coil, its "magnetic volume", to be  $(v/\lambda)$ .

The test model which we have built for the receiver has  $\gamma$  set much less than unity because we did not feel that we needed to utilize all the energy gain that the antenna was capable of providing. As long as the intrinsic antenna noise dominated the SQUID's intrinsic noise, the match would be sufficient. Better coupling would only serve to decrease the dynamic range of the receiver by "over driving" the SQUID. The details of our matching transformer will be discussed more fully in Section 3.3.

### 2.3 Cryostat Dissipation

Thermal noise currents which flow in any conductive materials in the cryostat can inductively couple magnetic noise into the antenna. We had originally proposed that we would perform calculations to determine the magnitude of this effect. However, when we began doing calculations based on simplified models for the superinsulation



and its interaction with the transversely oriented pickup loop, we realized that we would not have very much confidence in our results.. The necessary simplifications were simply too extreme.

Our solution to the problem was to make a room temperature mock-up of the full scale induction coil and resonate it at 3 kHz or above. We could then accurately monitor the Q factor of this coil when in free space and when enclosed in blankets of superinsulation or thermal shields such as would be used in a cryostat.

By measuring changes in the coil Q due to nearby materials, we determined the effective resistance  $R_{eq}$  which was added into the antenna circuit. In Appendix D we show that

$$R_{eq} = M^2 \omega^2 / R_D \quad (2.3.1)$$

where M is the mutual inductance between the tank coil and the external dissipative material,  $\omega$  is the angular frequency and  $R_{ext}$  is the loop resistance of the external material. Since we can assign a fairly accurate temperature to these materials, we can predict from these measurements just how much noise would be coupled into an actual antenna. In Appendix D we have worked out this correspondence explicitly. The result is simply that dissipative dewar materials at a temperature  $T_D$  can be represented by an equivalent resistance  $R_{eq}$  which generates a noise voltage

$$V_n / \sqrt{Hz} = (4k_B T_D R_{eq})^{1/2} \quad (2.3.2)$$

#### 2.4 SQUID and SQUID Control Electronics

For all of our measurements, whether operating at bias (pump) frequencies of 60 or 150 MHz, we have used completely unmodified Model TSQ sensors. These are toroidal, point-contact devices. At these operating frequencies, intrinsic SQUID noise in the devices is found to be negligible compared to amplifier noise.

Tests conducted during the first part of this project used a 60 MHz electronics package, somewhat similar to our commercial Model 30 SQUID controller. One important advance, however, was the inclusion of all feedback circuits in the controller's "head", a modification which permitted faster slewing. This instrument still used a high Q resonant rf line to the SQUID and simple video detection of the 60 MHz signal.

We later switched to a higher pump frequency, 150 MHz, in order to obtain a matched  $50 \Omega$  transmission line between the SQUID and the "head". This 150 MHz system also contained all feedback components in the head and utilized homodyne rather than video detection. The reason for this change is two-fold. First, it improved noise immunity, and second, it improved open loop gain stability by making the detector insertion loss a well-defined quantity. The details of the control unit are covered in Section 3.4.

## 2.5 Feedback Considerations

There are two distinct feedback paths used in this receiver. The first is the conventional feedback used to lock a SQUID detector onto a signal quantum and linearize its response. In the second path shown in Fig. 2.1, we take a current proportional to the output voltage and inject it into a loop which is coupled to the antenna induction coil. The effect of this feedback is to reduce the apparent  $Q$  of the receiver from the natural  $Q$  of the antenna circuit ( $\sim 10^3$ ) to around 10 or less, and thereby increase the 3 dB bandwidth to a more practical value.

### 3. DESCRIPTION OF COMPONENTS

#### 3.1 Dissipation Test Inductors

These are rather large, toroidally wound inductors which have been used to estimate the Q factor which we could expect to obtain from a full scale antenna induction coil. The coil forms were machined from G-10 fiberglass tubes and plates, and assembled with epoxy adhesive. They are 30.5 cm long, with an inner diameter of 5.1 cm and an outer diameter of 15.2 cm. The tubes are 0.3 cm thick and the plates are 0.6 cm thick. After assembly, the toroids were cut symmetrically in a plane parallel to their principal axis. This was done to facilitate winding. After winding them with superconducting wire the two halves were bound back together with dacron fishing line.

Two toroids were actually wound and tested. Originally, we had planned to test four different types of wire, but the first two inductors performed so far above the minimum requirements that we deemed further work unnecessary.

The first toroid (T1) was wound in a single layer with 600 turns of 0.025 cm diameter Nb-Ti wire (Supercon, type T48). The second (T2) was similarly wound with 600 turns of 0.025 cm diameter multifilament copper clad Nb-Ti wire (Supercon, type V.S.F.). The length of wire in each coil was about 420 meters, and the enclosed volume was approximately 5000 cm<sup>3</sup>.

#### 3.2 Dissipation Test Capacitors

Each capacitor was constructed from 0.025 mm lead foil and 0.012 mm mylar foil. Two strips, 6 cm wide by 70 cm long, were cut out of each material. They were then arranged in an alternating stack and rolled tightly on a 1.3 cm diameter fiberglass rod. The two lead strips were displaced laterally from the mylar so that an exposed edge of each piece was available at each end of the assembly. Copper leads were soldered to this exposed edge. A single layer of dacron fishing line was then tightly wound around the entire structure. Those capacitors which had not become shorted during assembly appeared able to withstand subsequent thermal cycling with no ill effects. The capacitance of these components would reversibly drop by about 15% upon cooling to 4.2 K. The capacitor actually used in the antenna dissipation test had a 4.2 K value of 0.11  $\mu$ F.



### 3.3 Dissipation Test Probe

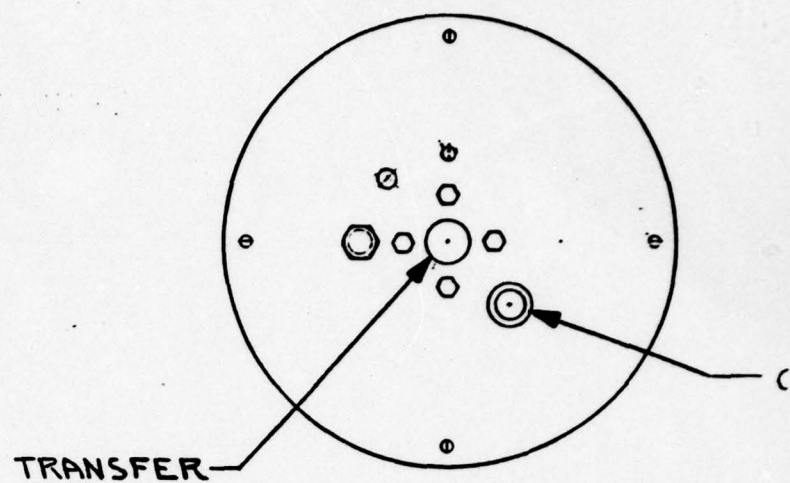
This component provided a rigid, magnetically shielded environment for a test inductor, capacitor, and transformer. Shown in Fig. 3.1, the two-piece probe was designed to fit into an existing 20 cm access helium cryostat. Its lead covered bucket remained in the bottom of the cryostat and its removable insert held a test inductor and capacitor. This insert could be clamped very rigidly into the bucket by means of a large anchoring screw visible in Fig. 3.1. A fiberglass mounting plate at the bottom of the insert held the toroidal inductor and the resonating capacitor. All metals used inside the shielded region were superconducting at 4.2 K.

We placed a superconducting decoupling transformer in series with the toroid and capacitor. This arrangement allowed us both to excite and to monitor the tank circuit. The transformer had 250 turns of 0.13 mm diameter Nb-Ti wire (Supercon, type T48) for the primary and secondary. They were wound on a 1.3 cm diameter  $\times$  2.5 cm long fiberglass bobbin. Each winding had an inductance of 250  $\mu$ H. The primary of this transformer coupled very weakly to the tank circuit so that losses in the monitoring instrument or the leads to it did not broaden the resonance. The secondary was connected to a jack on top of the probe through a stainless steel transmission line.

### 3.4 Cryostat Dissipation Test Fixtures

We fabricated a full scale mockup of the antenna induction coil using a plywood form as shown in Fig. 3.2. This form was wound with 202 turns of #28 copper wire, uniformly spaced as shown in the drawing. The inductance of this coil was 22 mH and its resistance was 85  $\Omega$  at room temperature. This assembly was not intended for cryogenic operation.

To provide a form on which to wrap superinsulation, we took a 100 cm length of 26 cm diameter fiberglass tubing and attached a plywood cap to one end. The end of a light rope was connected to the center of this cap and was passed over a pulley on the ceiling so that we could easily raise and lower the cylindrical form. The mock induction coil was placed on a 60 cm high pedestal directly under this fiberglass cylinder so that the cylinder could be dropped over and lifted off the coil. As we described in Section 4.4, this apparatus allowed us to perform a "chopped" measurement of the dissipative effects of any material wrapped on the cylinder.



TE

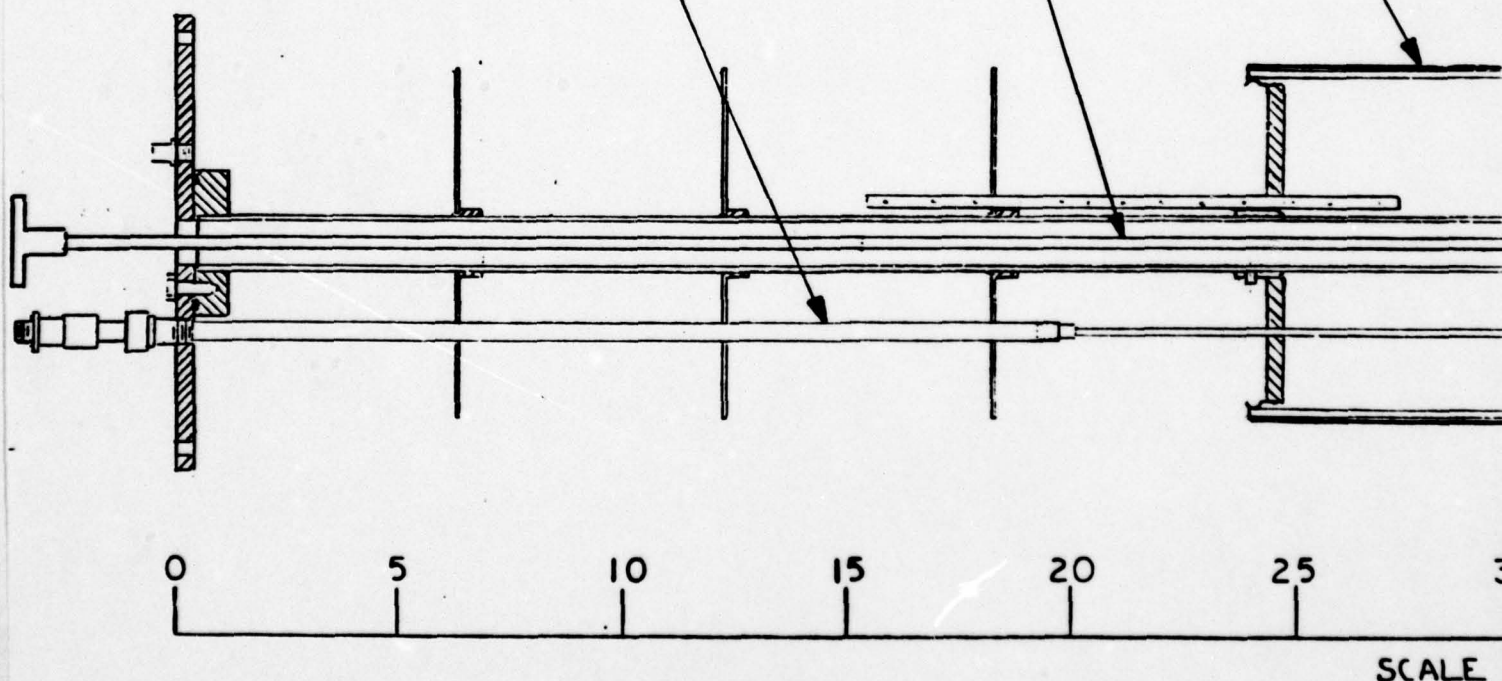
DECOL  
TRAN

REMOVABLE  
"NUT DRIVER"

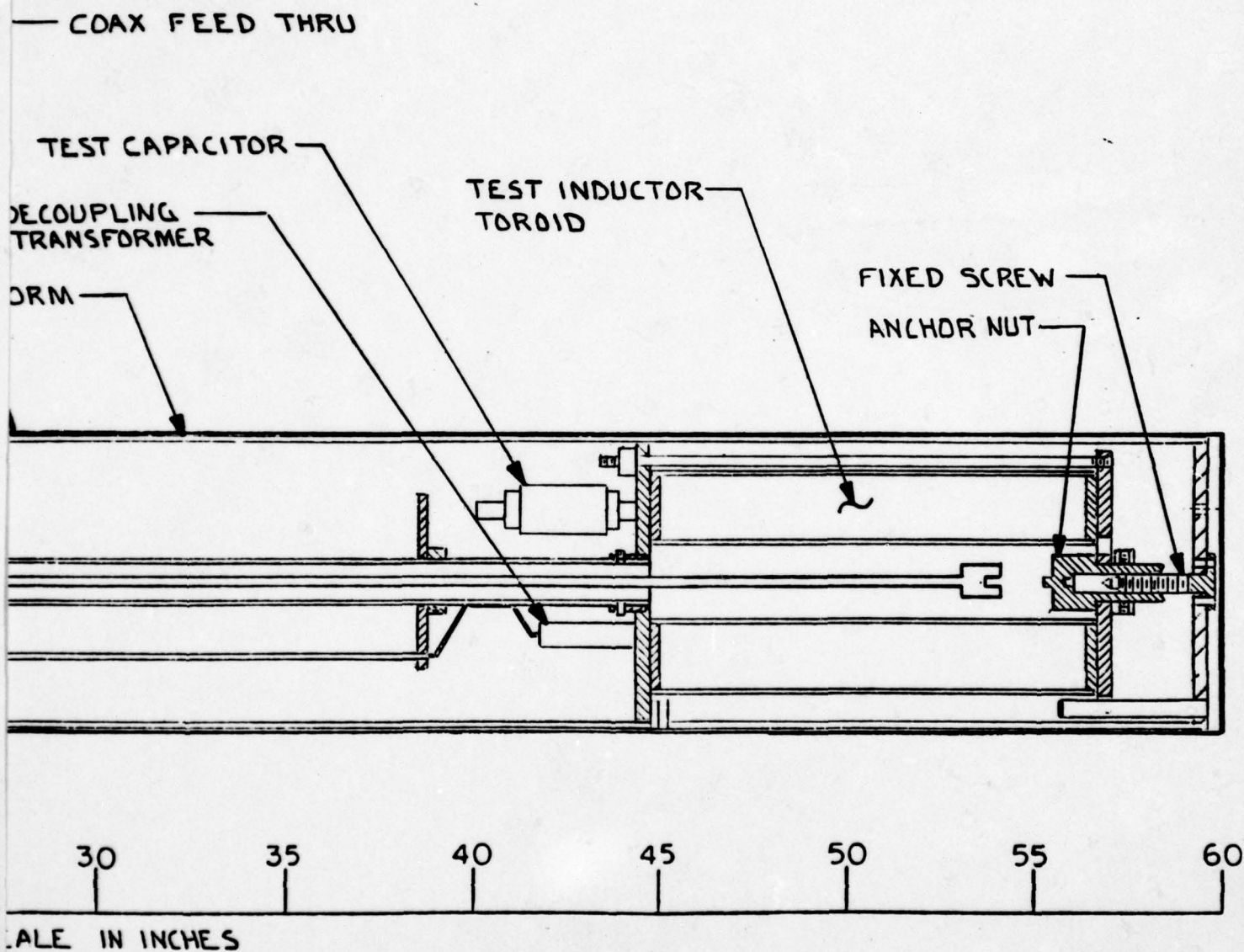
TRANSMISSION LINE

FIBERGLASS FORM

LEAD SHEET



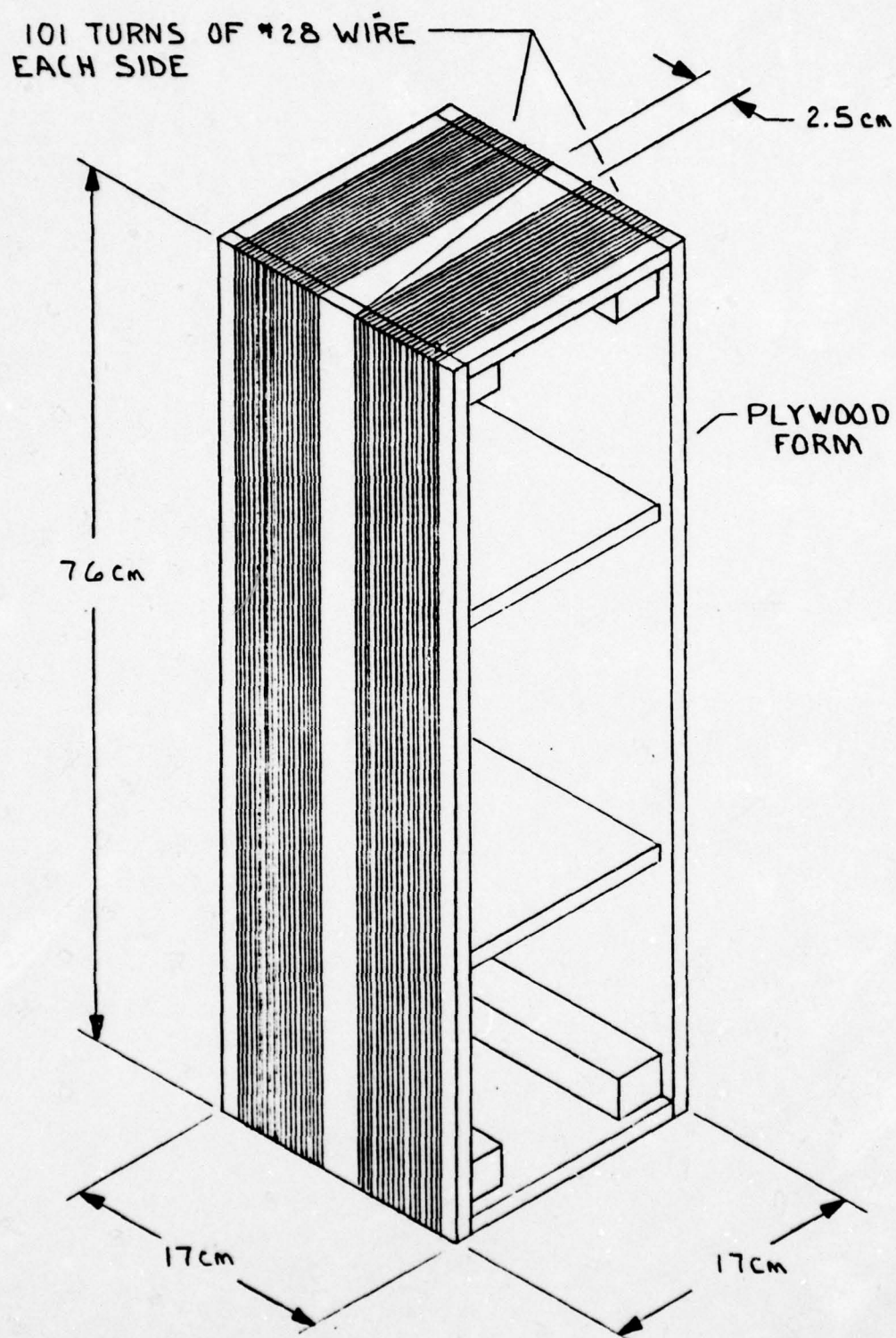
Left on two pages



DISSIPATION TEST PROBE  
FIG 3.1

*Right of 2 pages  
this side on top*





MOCKUP OF FULL SCALE ANTENNA INDUCTION COIL

FIG 3.2

A 26 cm diameter thermal radiation shield was also rigged so that it could be similarly lowered over the induction coil. It was constructed using our standard proprietary design for electromagnetically transparent shields. Their high thermal conductivity is obtained from an array of non-intersecting aluminum wires imbedded in a reinforced epoxy matrix.

### 3.5 Model Receiver Test Probe

Most of the specifications of the model receiver were determined using this probe, which was designed to fit into the 5 cm diameter neck of our 50 l storage dewar. The layout and construction of this probe are shown in Fig. 3.3.

At the bottom end of the probe we have wound a superconducting capacitor identical to the "dissipation test capacitor" described in Section 3.2. Its capacity at 4.2 K was measured to be 0.125  $\mu$ F, 15% less than its room temperature value.

Directly above the capacitor, on the same fiberglass support rod, we wound a "model" induction coil. This coil comprised 1890 turns of 0.13 mm Nb-Ti wire (Supercon, type T48). The number of turns on the coil was selected by trial and error to give a resonance at 3.00 kHz when placed in series with the capacitor and the transformer described elsewhere in this section. The coil was randomly wound and then wrapped tightly with several layers of mylar tape to protect it and make it more rigid. The inductance was measured at 4.2 K using a Hewlett-Packard Model 4260A bridge and found to be 21.1 mH.

We wound the matching transformer about 3 cm above the top of the induction coil, also using Supercon T48 wire for both primary and secondary. We wrapped two insulated turns of 0.025 mm lead foil over the primary of this transformer before winding on the secondary. This foil was then connected to the housing of the SQUID, and served as an electrostatic rfi shield between the primary and secondary. Although not necessary for this test probe, such a shield would probably be needed with a full sized induction coil operating in an unshielded environment.

The design inductances for this transformer were calculated using the equations developed in Appendix C in addition to the information that the SQUID inductance,  $L_S$ , was 2.0  $\mu$ H and the desired coupling inductance,  $L_C$ , was 2.5 mH. The only additional piece of data required to determine the optimum inductances was the

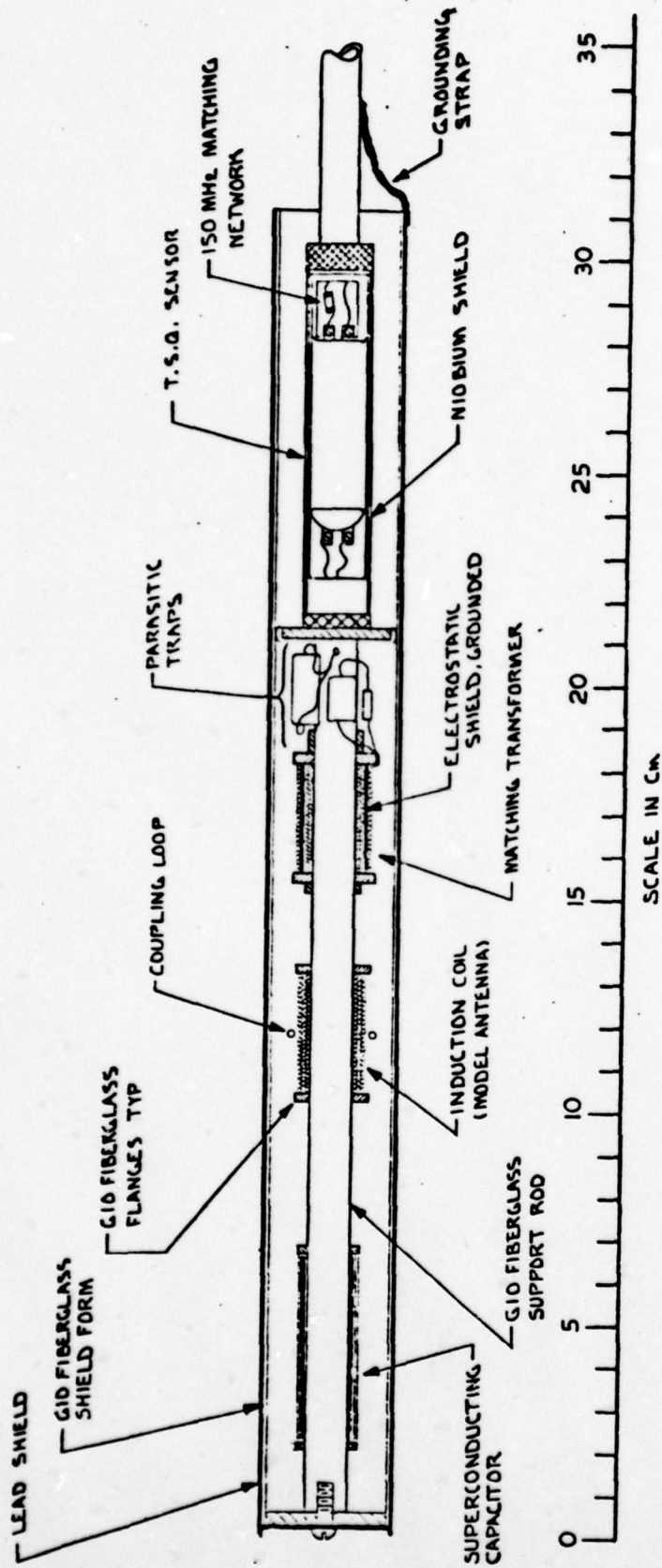


FIG 3.3

| TITLE   |                      | TOLERANCES<br>SPECIAL SYMBOLS |      | MATERIAL                 |                     |
|---|----------------------|-------------------------------|------|--------------------------|---------------------|
| MODEL RECEIVER PROBE<br>MECHANICAL CONSTRUCTION |                      |                               |      | FINISH                   |                     |
|   |                      |                               |      | DRN. BY DATE<br>3 4-7-78 |                     |
| S.H.E. CORPORATION<br>SAN DIEGO, CALIFORNIA     |                      | DIMENSIONS                    |      | APPR'D BY DATE           |                     |
|   |                      |                               |      | SCALE                    |                     |
| SYM.  | REVISION DESCRIPTION | BY                            | DATE | SHEET 1 OF 1             | ASSY. DWG.          |
|   |                      |                               |      |                          | DWG. NO. A 2000-259 |
|   |                      |                               |      |                          | REV.                |



coupling coefficient  $K$ . This was estimated to be 0.9 from our experience with other similar transformers.

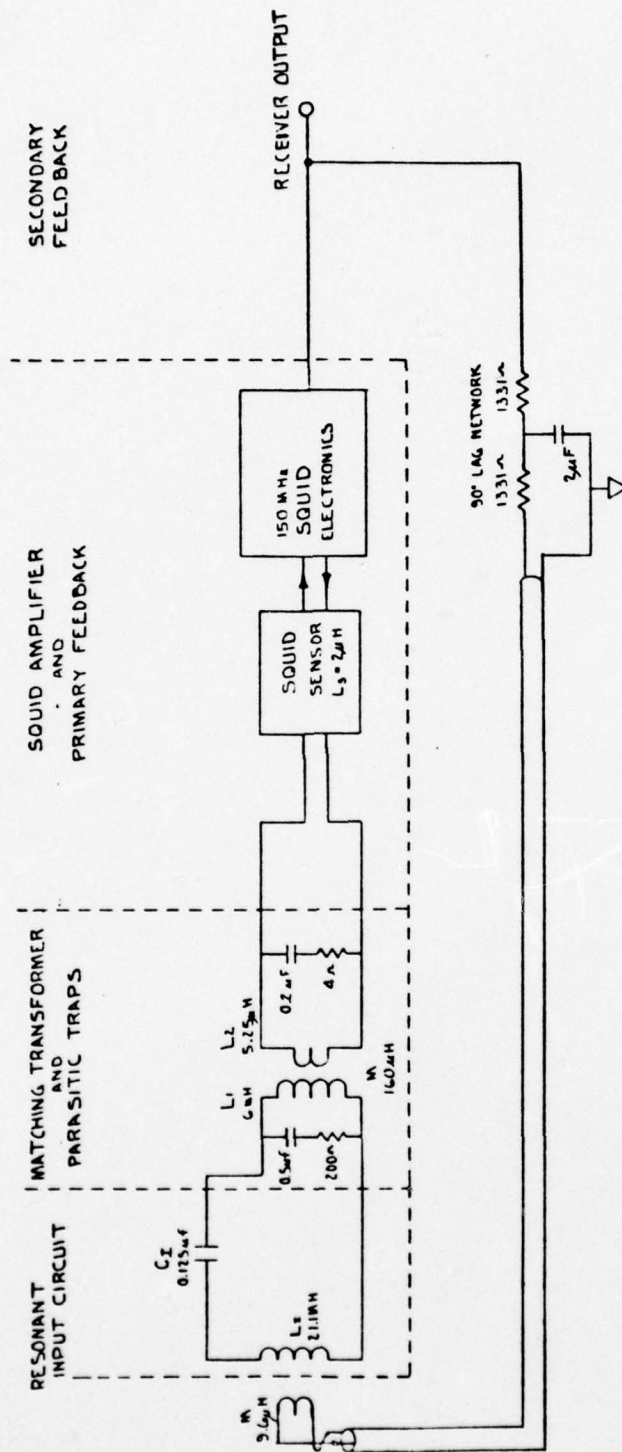
The 6 mH primary required 1000 turns closely wound over a 2.5 cm length while the 5.25  $\mu$ H secondary took 29 turns spaced uniformly over this same length. The actual coupling coefficient of this transformer was determined by measuring the apparent inductance of the primary with the secondary both shorted and opened, since the ratio of these two values is equal to  $(1 - K^2)$ . We measured  $K$  to be 0.92 so that our design, in its first approximation, was suitably self-consistent.

We calculated the resonant frequency of this model receiver by solving  $\omega(L_I + L_C) = 1/\omega C_I$ . The resulting frequency was 2943 Hz.

We found it necessary to install the R-C network shown in Fig. 3.4 across the primary of the matching transformer. Without this trap, the quantum interference pattern of the SQUID was barely visible and was extremely noisy. The capacitor value was chosen to roll off the transformer above 14 kHz, while the resistor kept the  $Q$  of the circuit low to prevent resonance problems. This trap, and one similarly conceived, across the SQUID input coil dramatically improved the performance of the receiver system. Apparently they suppressed parasitic oscillations being driven by the SQUID.

The SQUID was mounted in a niobium shielded cylinder above the matching transformer and other antenna components. Apart from the matching network between the transmission line and the tank coil of the SQUID, there was nothing special about the electrical or mechanical connections to this TSQ sensor. The SQUID and housing were both standard commercial units. The series inductor and shunt capacitor in the pump circuit were chosen, using a Smith chart, to transform the tank impedance into a real 50  $\Omega$  at resonance. Because of this matching condition, one can locate the proper operating frequency by using a sweep generator to find a sharp dip in the power reflected from the SQUID. We have constructed a wideband video amplifier for this purpose. This video amplifier has also been useful in scanning the pump circuit for spurious resonances and other malfunctions.

The current sensitivities of the input and rf coils of this SQUID were measured to be  $1.04 \times 10^{-7}$  A/ $\phi_0$  and  $1.05 \times 10^{-6}$  A/ $\phi_0$ , respectively. We have also measured the input coil inductance to be  $2.0 \times 10^{-6}$  H for this type of SQUID.



MODEL RECEIVER - SUBSYSTEM SCHEMATIC

FIG 3.4

We wrapped a single turn loop around the outside of the test probe induction coil and connected it to the top of the probe by a shielded twisted pair of #36 copper wires that terminated in a SMA coaxial connector. This coupling loop provided a means of injecting signal and feedback voltages directly into the induction coil circuit. As discussed in Section 4.2, we determined the mutual inductance between this coupling loop and the induction coil by measuring voltage induced in the induction coil due to a measured current in the coupling loop. This was done at 1.5 kHz, and 6.0 kHz with the coil at 4.2 K. These measurements all gave  $M = 9.6 \mu\text{H}$ .

### 3.6 SQUID Electronics

In Fig. 3.5 we show a block diagram of the 150 MHz SQUID control system. In a final version of this control unit, all the components shown in Fig. 3.5 would be mounted in a small package near the cryostat. In our breadboard version, the 150 MHz oscillator, the 10 dB directional coupler, and the variable attenuation were actually separate "connectorized" components connected to the control unit by coaxial cables.

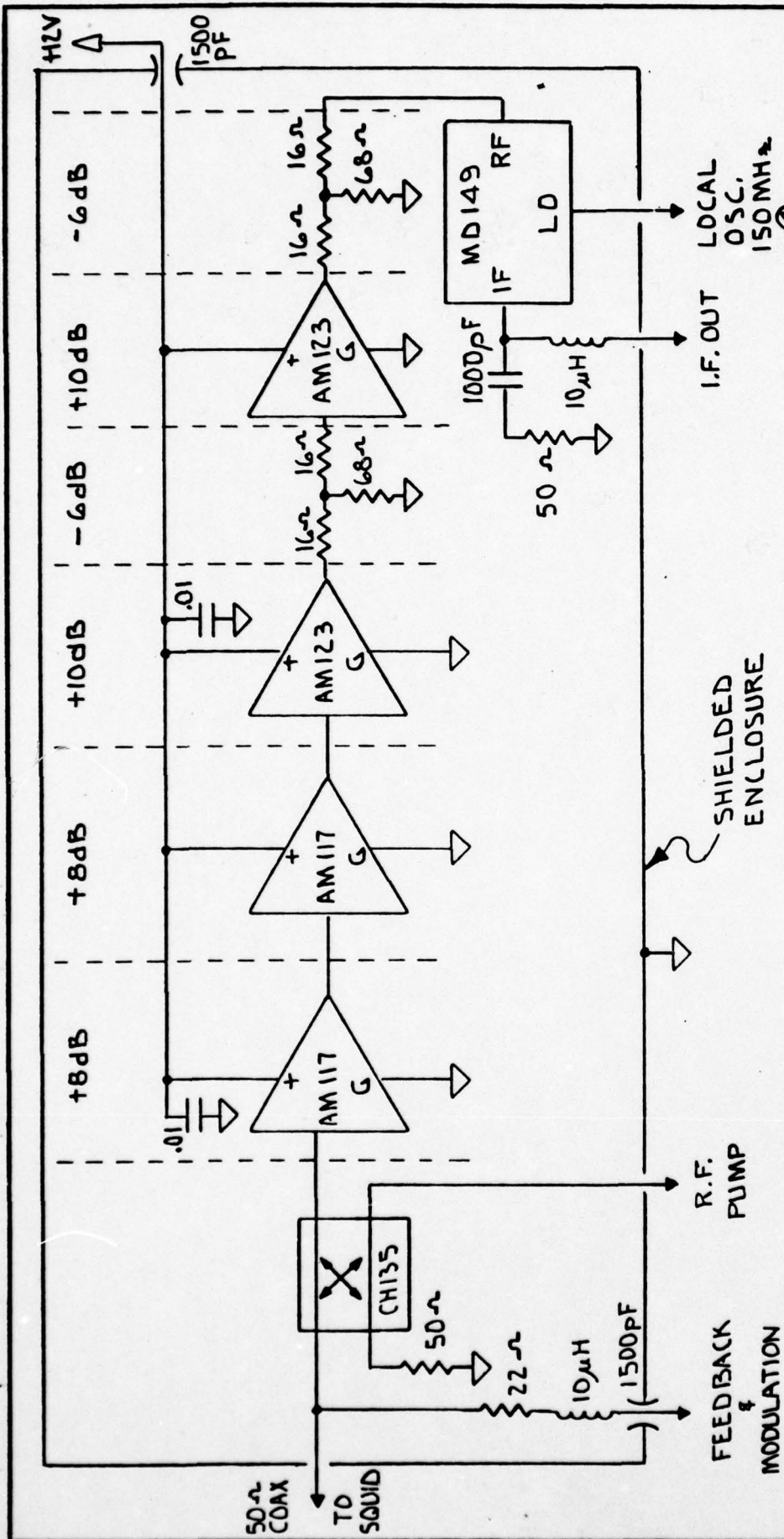
The components enclosed in the dashed line and labeled VHF subsystem were all housed in a machined aluminum box which had an rf-tight lid. Power and feedback signals were introduced into the box via 1500 pF feedthrough capacitors, while rf signals were introduced through SMA connectors. Additional shunt capacitance and series inductance were found to be necessary in the power supply line to provide adequate decoupling between the VHF stages and the remainder of the control unit.

The internal details of the VHF subsystem are shown in Fig. 3.6. Each of the Anzac components was mounted directly on the copper clad surface of a piece of circuit board. This surface formed a convenient ground plane for the circuit since the numerous ground leads on the Anzac "flat packs" could be soldered directly to this copper sheet.

The directional coupler (CH 135) permitted us to channel pump power selectively to the SQUID so that device could be operated in the reflection mode. The two 6 dB attenuator pads were designed into the amplifier chain to increase the reverse isolation between the mixer and the SQUID. The effective forward and reverse power gains for this chain of amplifiers were 24 dB and 65 dB, respectively.





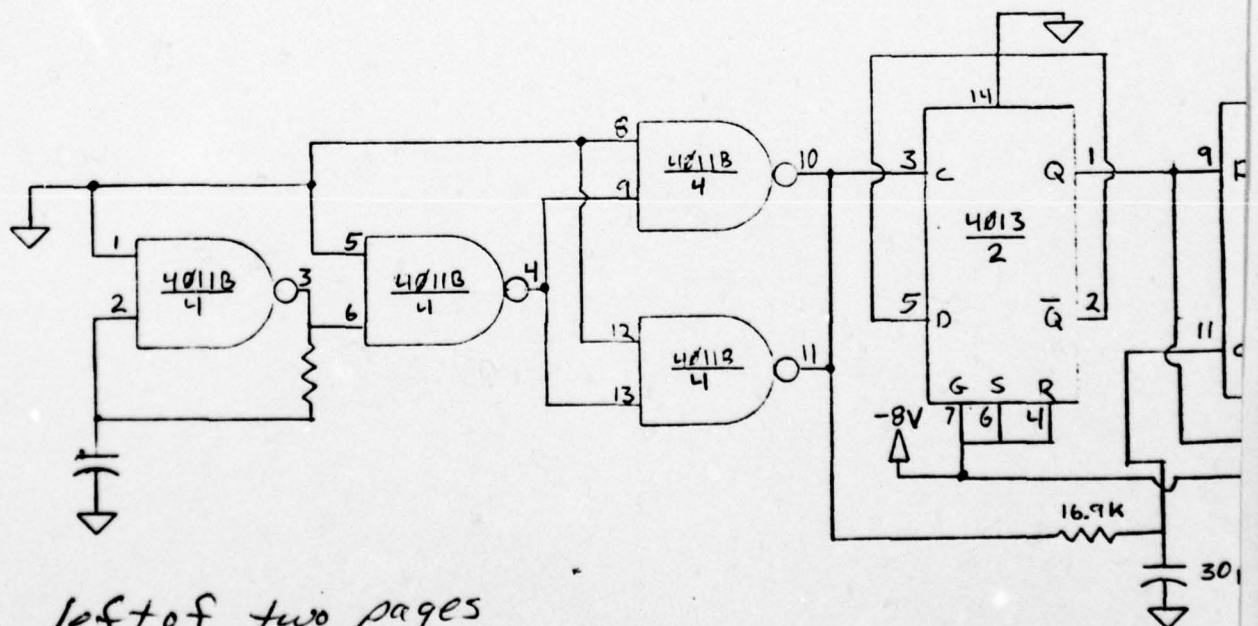
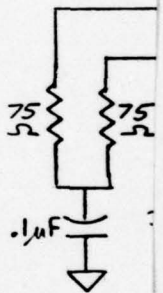
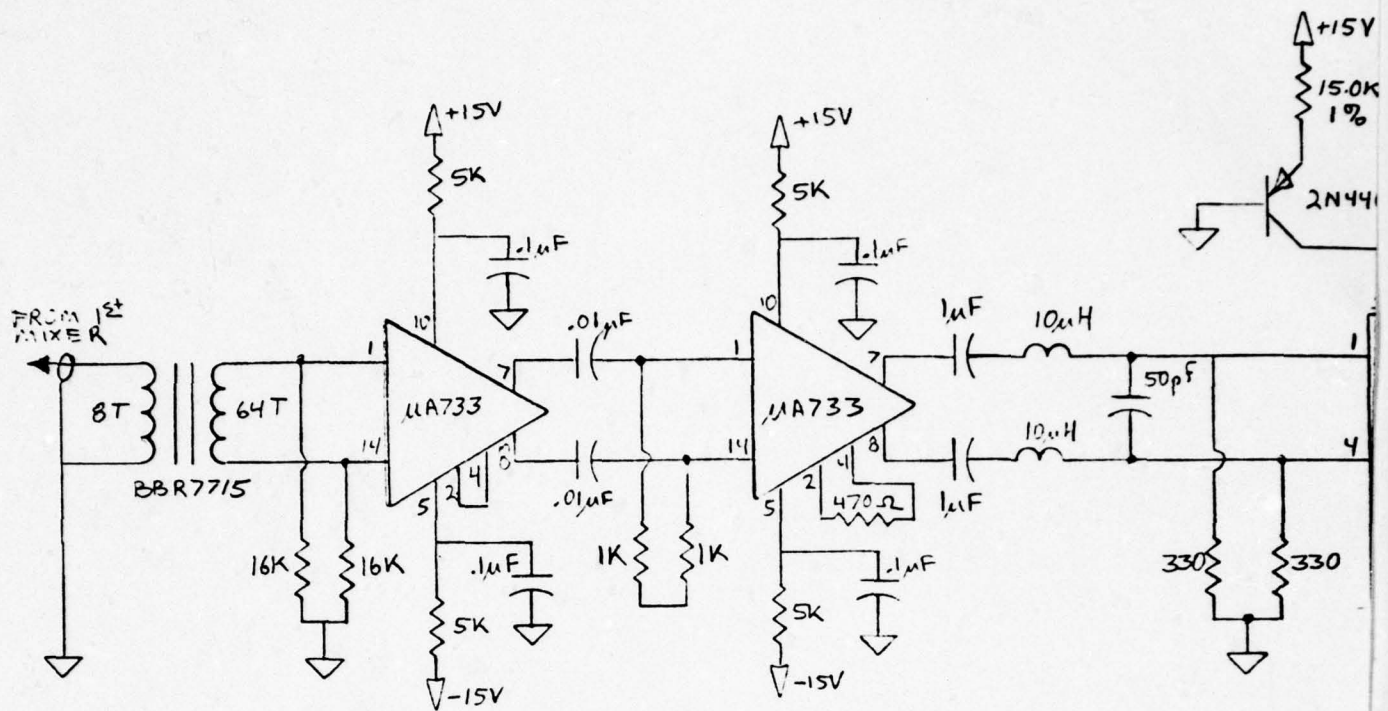




NOTE: ALL PART NUMBERS  
REFER TO "ANZAC" DEVICES

FIG 3.6

| MATERIAL   |  | TOLERANCES<br>SPECIAL SYMBOLS |  | TITLE   |  |
|--|--|-------------------------------|--|---|--|
| FINISH   |  |                               |  | VHF AMPLIFIER CHAIN<br>FOR 150 MH± SQUID AMPLIFIER  |  |
| DRN. BY<br> |  | DATE                          |  | <br><b>S.H.E. CORPORATION</b><br>SAN DIEGO, CALIFORNIA |  |
| APP'D BY   |  | DATE                          |  |   |  |
| SCALE  |  | DIMENSIONS                    |  | ASSY. DWG.  |  |
| REVISION DESCRIPTION   |  | BY                            |  | DWG. NO.  |  |
|  |  |                               |  | A2000-273   |  |
| SYM.   |  | DATE                          |  | REV.  |  |



left of two pages  
This side on top



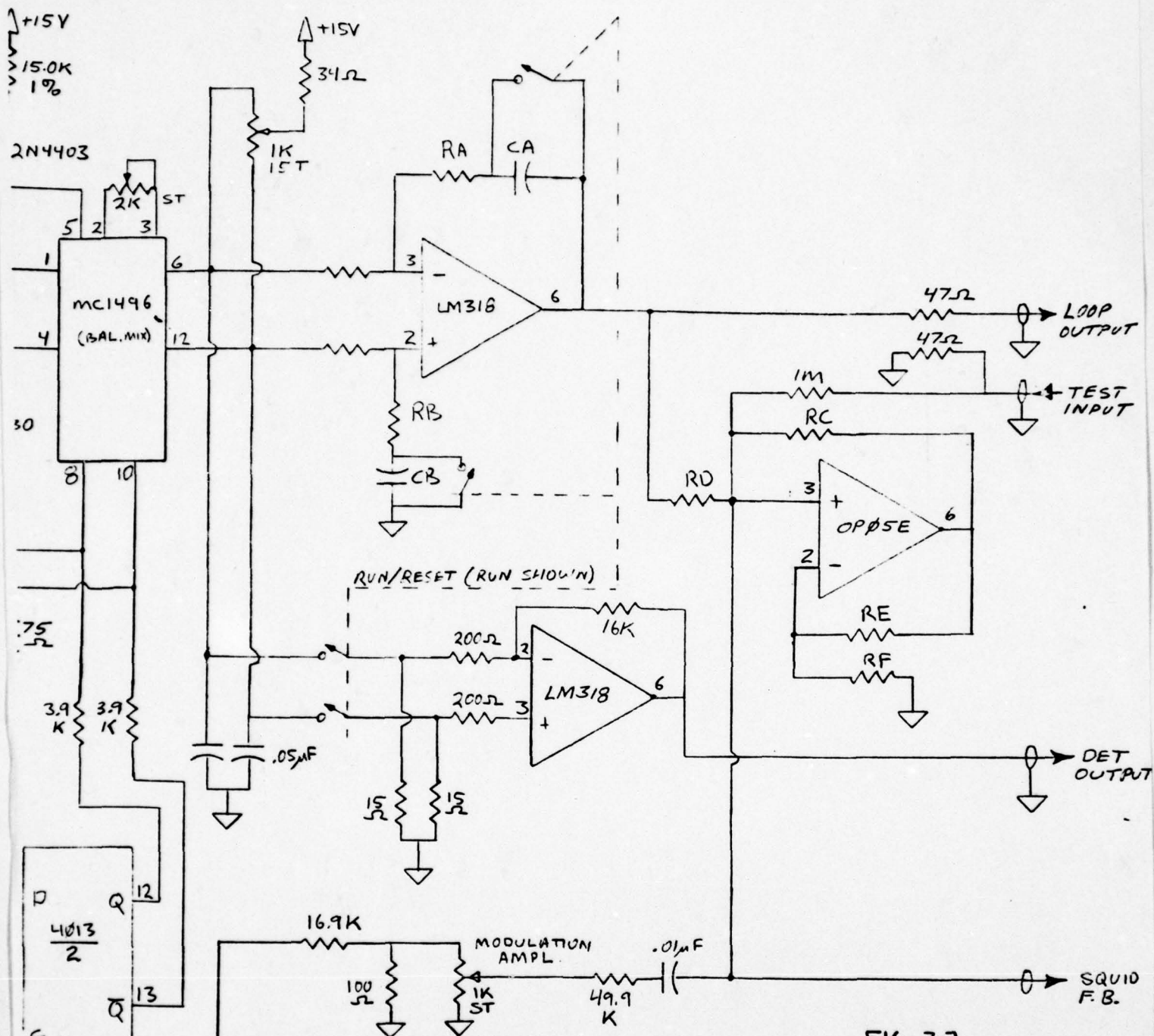




FIG 3.7

|      |  |  |   |  |                               |  |  |  |  |  |
|------|--|--|---|--|-------------------------------|--|--|--|--|--|
| 8 17 |  |  | MATERIAL  |  | TOLERANCES<br>SPECIAL SYMBOLS |  | TITLE<br>FEEDBACK BOARD FOR<br>150 MHz SQUID AMPLIFIER |  |  |  |
|      |  |  | FINISH  |  |                               |  |  |  |  |  |
| PF   |  |  | DRN BY<br> |  | DATE                          |  |  |  |  |  |
|      |  |  | APPV'D BY   |  | DATE                          |  | DIMENSIONS   |  |  S.H.E. CORPORATION<br>SAN DIEGO, CALIFORNIA |  |
| TION |  |  | BY  |  | DATE                          |  | SCALE  |  | SHEET 1 OF 1   |  |
|      |  |  |   |  |                               |  |  |  | ASSY. DWG.   |  |
|      |  |  |   |  |                               |  |  |  | DWG. NO.<br>B2000-215  |  |
|      |  |  |   |  |                               |  |  |  | REV.   |  |

Right of Two pages

The mixer, when operated at a local oscillator (L.O.) level of +3 dBm had a conversion loss of 5.8 dB at 150 MHz. This implied an overall power gain at the input to the I.F. amplifier of 18.2 dB. The reverse isolation between the L.O. and rf ports was typically 40 dB, so that the power transferred backward from the local oscillator to the SQUID was about -100 dBm. This was comfortably less power than that required to bias our SQUID to its operating point at this frequency. This was an important consideration since a spurious rf bias from the L.O. would cause problems both in setting the correct bias level and in optimizing the relative phase of the L.O.

The overall noise figure of the VHF amplifier and the mixer was both calculated and measured to be 1.8 dB. This rather good performance was due to the use of two 1.5 db noise figure Anzac AM117 amplifier modules for the input stages.

The I.F. stages, modulator, second mixer, and feedback components were all mounted on a 12 cm x 13 cm prototyping board which fit into the head enclosure. The circuitry contained on this board is shown in Fig. 3.7. The 500 kHz modulation signal for the SQUID was generated by the 4011 and 4013 CMOS devices. The two  $\mu$ A733 integrated video amplifiers boost the 500 kHz signal coming from the first mixer and present it to the second mixer. This second mixer was a very fast integrated device which used current steering logic. The completely demodulated output then went to a resetable integrator and became the primary feedback signal for operating the SQUID in a closed loop mode. The OP-05 amplifier was configured as a bootstrap circuit to improve the ability the feedback resistor  $R_F$  to act as a voltage to current converter. This resistor was selected so that with the feedback connected, the gain of the SQUID amplifier was  $3.3 \times 10^6$  volts per ampere into the SQUID input coil. This gain can be written as an impedance

$$Z_G = V_O/I_S = 3.3 \times 10^6 \Omega \quad . \quad (3.6.1)$$

The flux quantum resolution of this SQUID/amplifier system was measured to be  $5 \times 10^{-5} \phi_0/\sqrt{\text{Hz}}$ . In terms of energy sensitivity this is  $2.5 \times 10^{-29}$  J/Hz.

The prototype control electronics were housed in an aluminum box measuring 14 cm x 16 cm x 4.3 cm. Although the 150 MHz oscillator, directional coupler, and variable attenuators were not actually mounted in this enclosure, there was room available for each of these devices. We expect that a "production" version

of this controller head would be approximately the same size. The only support circuitry needed with such a production head would be a  $\pm 15$  V, 5 W power supply and some provision for applying the proper control voltages to set the rf bias level and frequency.

### 3.7 Secondary Feedback

The receiver output goes to the lag network shown in Fig. 3.4. The current out of this lag network flows through a coupling loop wrapped around the induction coil. Above  $\omega \approx 10^3$ /sec, the network behaves in this circuit like a series inductor  $L_F = 3.5$  H, so its effective transfer impedance can be written as  $Z_F = \omega L_F$ . Since the mutual inductance between this loop and the induction coil is  $M_c = 9.6 \mu\text{H}$ , we can find  $V_I$ , the voltage induced in the antenna circuit for a given receiver output voltage,  $V_o$ . Specifically,

$$G_F = \frac{V_I}{V_o} = \frac{M_c \omega}{Z_F} = 2.74 \times 10^{-6} \quad (3.7.1)$$

This equation gives the voltage loss ratio in the feedback path, which we may multiply by the forward voltage gain of the receiver to get the net gain for the feedback loop. In the frequency range where this net gain is much greater than unity, the secondary feedback will dominate the closed loop response of the receiver and cause it to be flat. Standard circuit analysis shows that for this circuit the 3 dB points of the frequency response should occur when the magnitude of the net gain is unity. We can calculate the forward voltage gain from Eq. 2.2.2 if we note that

$$V_I = \omega N A B_{\text{ANTENNA}} .$$

The magnitude of net gain around the feedback loop is then found by combining Eq 2.2.2, Eq 3.6.1, and Eq 3.7.1.

$$G_N = \left( \frac{L_I}{L_S} \right)^{1/2} \left( \frac{\gamma^{1/2}}{1 + \gamma} \right) \left( \frac{Z_G}{Z_F} \right) \left( \frac{M_c}{L_I} \right) \left( \frac{\omega}{2\Delta\omega} \right) \left( \alpha^{1/2} \right) . \quad (3.7.3)$$

Setting  $G_N = 1$  we can evaluate this equation to find that the calculated 3 dB bandwidth  $2\Delta\omega$ , is 1400 Hz. The apparent Q would be 2.14 with the external feedback connected.



## 4.1 DESCRIPTION OF TESTS AND RESULTS

### 4.1 Frequency Response of Model Receiver

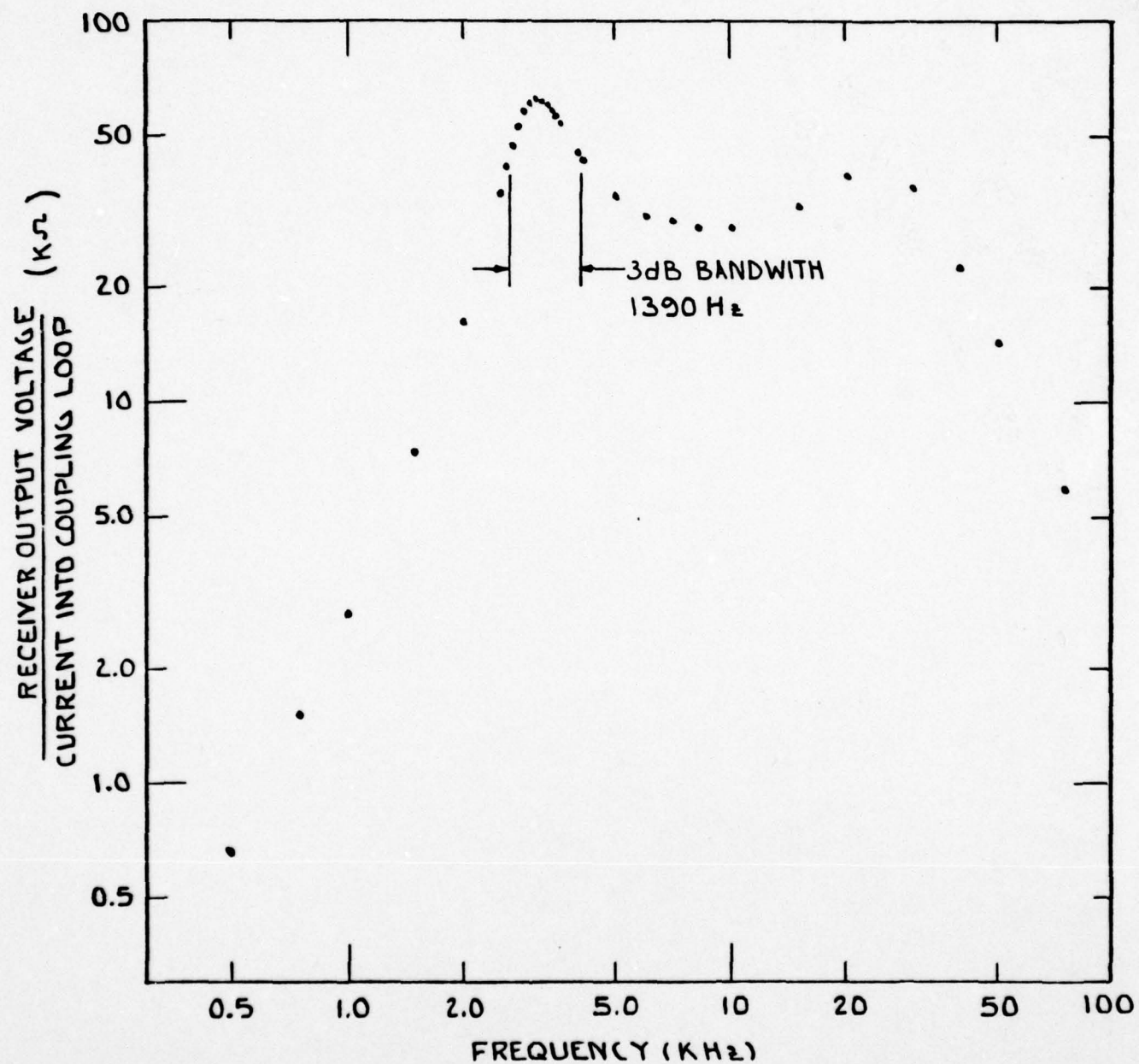
We used a Princeton Applied Research (P.A.R.) Model 124 phase sensitive amplifier, a Hewlett-Packard Model 3465A digital multimeter, and a Ballantine Model 5500A counter in this measurement.

The receiver was operated with both primary and secondary feedback connected. A signal current was run directly into the coupling loop around the antenna induction coil. This signal was obtained, through a 1 K ohm dropping resistor, from the output of the reference channel of the P.A.R. amplifier. The amplitude of this drive signal was monitored using the ac current measuring capability of the Hewlett-Packard multimeter. The output of the receiver was run through a 100:1 attenuator to the signal input of the P.A.R. amplifier.

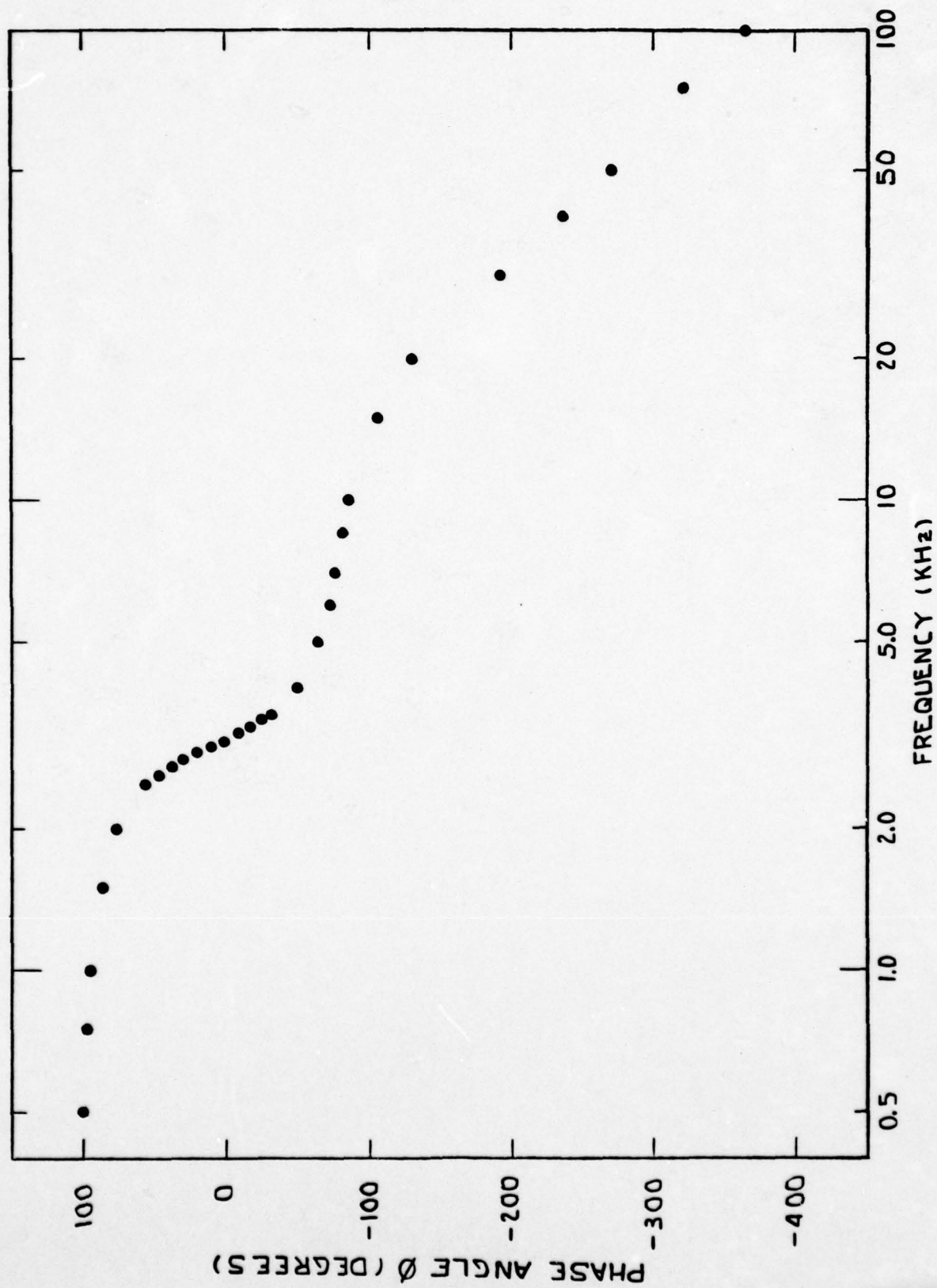
The reference channel frequency was set to the resonant frequency of the receiver by tuning for a maximum output. The phase of the output was arbitrarily defined to be zero degrees at this frequency. The amplitude of the input signal was chosen so that the output voltage was kept around a few volts except that far above resonance, reduced amplitudes were required to prevent unlocking of the SQUID electronics. The Ballantine counter was used to accurately measure each frequency at which data were taken. The data consisted of the input current amplitude, the output voltage amplitude and the output voltage phase. These data have been reduced into the graphs of Fig. 4.1 and Fig. 4.2.

The frequency response shown in Fig. 4.1 is distorted from a natural Q curve by two factors. First the voltage induced in the antenna is proportional to frequency for a given drive current, so the entire graph is tilted. Second, the primary feedback path has some low-pass compensation at 10 kHz which causes a pronounced peaking of the receiver response.

The shape of the response shown in Fig. 4.1 is the same as that which would be obtained from a constant amplitude magnetic field applied to the induction coil. The accentuation of high frequencies occurs in both cases.



GAIN VS. FREQUENCY FOR MODEL RECEIVER  
FIG 4.1



PHASE VS. FREQUENCY FOR MODEL RECEIVER  
FIG 4.2



The measured 3 dB bandwidth of the receiver under these conditions was 1390 Hz and the peak response was at 3100 Hz. Due to the two skewing effects, the peak was not symmetrically placed in the passband. If the system output is divided by frequency to remove the "tilt", we get a frequency response which is much closer to a simple resonance curve. The apparent bandwidth decreases to 1200 Hz under these conditions, and the resonant frequency drops to 2995 Hz. These last two figures are the ones which should be compared to the bandwidth and resonant frequency calculated in Sections 3.5 and 3.7.

#### 4.2 Gain of Model Receiver

We used a Hewlett-Packard Model 200 CD oscillator for the signal source and a Tektronics Model 7403N oscilloscope to measure the peak-to-peak input and output voltages. The signal frequency was measured with a Ballantine Model 5500 A counter.

The oscillator was connected to the input of the lag network and the output of the lag network was connected to the external coupling loop. The receiver was operated with the secondary feedback disconnected. We measured the amplitude of the signal appearing at the receiver output for a given signal voltage across the input of the filter network. This was done at the resonant frequency of the receiver and several frequencies near resonance. The data obtained are shown in Table 4.1.

Table 4.1 Receiver Voltage Gain Without Secondary Feedback

| Freq    | $\Delta\omega$ | $V_{in}$ | $V_{out}$ | $V_{out}/V_{in}$ |
|---------|----------------|----------|-----------|------------------|
| 2895 Hz | -100 Hz        | 0.50 V   | 3.0 V     | 6.0              |
| 2945    | -50            | 0.50     | 6.0       | 12.0             |
| 2965    | -30            | 0.10     | 2.0       | 20.0             |
| 2985    | -10            | 0.10     | 6.0       | 60.0             |
| 2995    | 0              | 0.005    | 5.7       | 1140.0           |
| 3005    | 10             | 0.10     | 6.0       | 60.0             |
| 3025    | 30             | 0.10     | 2.0       | 20.0             |
| 3045    | 50             | 0.50     | 6.0       | 12.0             |
| 3095    | 100            | 0.50     | 3.0       | 6.0              |

The gain versus frequency data exhibit the expected  $1/\Delta\omega$  response around resonance.

The finite gain of 1140 observed directly on resonance gives us, after normalization, a measure of the induction coil circuit Q factor. The normalized gain of the resonant circuit is  $\omega_0/2\Delta\omega$ , so that for  $\Delta\omega = 100$  Hz and  $\omega_0 = 2995$  Hz we would expect a gain of 15. Table 4.1 shows that our receiver had a gain of 6.0 under these conditions, so that normalization requires multiplying the table entries by 2.5. If we do this scaling to the gain on resonance we find that  $Q = 2850$  for our model receiver. From this Q factor we can obtain the thermal noise voltage in the antenna circuit, as discussed Appendix A. Combining Eq. A.2 and Eq. A.5 we find  $V_n = 6.0 \times 10^{-12} \text{ V}/\sqrt{\text{Hz}}$ .

We may compare our measured net gain with the value predicted from Eq. 3.7.3. This predicted gain is based on separate measurements of the properties of the induction coil, coupling loop, matching transformer, SQUID and SQUID electronics. At 100 Hz away from resonance this value is 7.0, about 16% higher than the measured net gain of 6.0 shown in Table 4.1. This 16% discrepancy is not unreasonable considering the number of separate measurements required to characterize the gain of the receiver.

We then measured the receiver gain with the secondary feedback connected by injecting a test current,  $I_C$ , into the coupling loop. At resonance we found that the gain between the coupling loop and the receiver output was  $6.3 \times 10^4 \text{ V/A}$ . From the current in the coupling loop and its mutual inductance with the induction coil we can immediately get the voltage generated in the antenna,  $V_I$ , using

$$V_I = M_C \omega I_C . \quad (4.2.1)$$

Taking  $M_C = 9.6 \text{ } \mu\text{H}$  and  $\omega = 1.88 \times 10^4$  gives our measured voltage gain at resonance to be  $3.48 \times 10^5$ . For a given induction coil volume and geometry this voltage gain can be written as a sensitivity in Volts/Gauss. In Section 5 we do this calculation in the specific case of our proposed full scale induction coil.

#### 4.3 Thermal Noise of Antenna

We used the test inductors, test capacitor, and test probe described in Sections 3.1 through 3.3. These were operated in a 20 cm access aluminum/fiberglass cryostat manufactured by Crogenics Associates. A Tektronics Model 7403N oscilloscope with Model 50C camera was used to record the decay rate of the tank

The finite gain of 1140 observed directly on resonance gives us, after normalization, a measure of the induction coil circuit Q factor. The normalized gain of the resonant circuit is  $\omega_0/2\Delta\omega$ , so that for  $\Delta\omega = 100$  Hz and  $\omega_0 = 2995$  Hz we would expect a gain of 15. Table 4.1 shows that our receiver had a gain of 6.0 under these conditions, so that normalization requires multiplying the table entries by 2.5. If we do this scaling to the gain on resonance we find that  $Q = 2850$  for our model receiver. From this Q factor we can obtain the thermal noise voltage in the antenna circuit, as discussed Appendix A. Combining Eq. A.2 and Eq. A.5 we find  $V_n = 6.0 \times 10^{-12} \text{ V}/\sqrt{\text{Hz}}$ .

We may compare our measured net gain with the value predicted from Eq. 3.7.3. This predicted gain is based on separate measurements of the properties of the induction coil, coupling loop, matching transformer, SQUID and SQUID electronics. At 100 Hz away from resonance this value is 7.0, about 16% higher than the measured net gain of 6.0 shown in Table 4.1. This 16% discrepancy is not unreasonable considering the number of separate measurements required to characterize the gain of the receiver.

We then measured the receiver gain with the secondary feedback connected by injecting a test current,  $I_C$ , into the coupling loop. At resonance we found that the gain between the coupling loop and the receiver output was  $6.3 \times 10^4 \text{ V/A}$ . From the current in the coupling loop and its mutual inductance with the induction coil we can immediately get the voltage generated in the antenna,  $V_I$ , using

$$V_I = M_C \omega I_C. \quad (4.2.1)$$

Taking  $M_C = 9.6 \text{ } \mu\text{H}$  and  $\omega = 1.88 \times 10^4$  gives our measured voltage gain at resonance to be  $3.48 \times 10^5$ . For a given induction coil volume and geometry this voltage gain can be written as a sensitivity in Volts/Gauss. In Section 5 we do this calculation in the specific case of our proposed full scale induction coil.

#### 4.3 Thermal Noise of Antenna

We used the test inductors, test capacitor, and test probe described in Sections 3.1 through 3.3. These were operated in a 20 cm access aluminum/fiberglass cryostat manufactured by Crogenics Associates. A Tektronics Model 7403N oscilloscope with Model 50C camera was used to record the decay rate of the tank



circuit and a P.A. R. Model 124 amplifier was used to measure its resonant frequency.

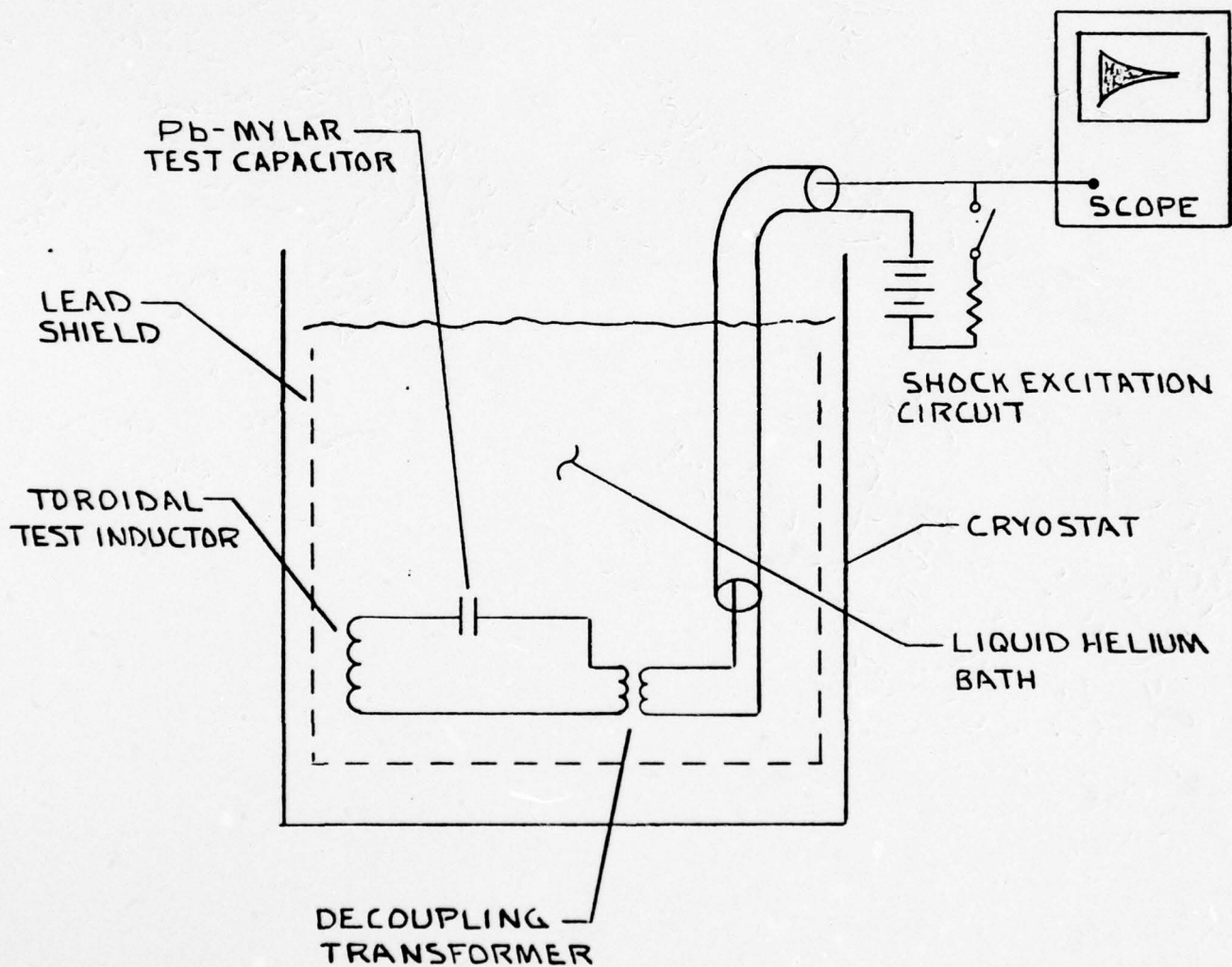
The inductor, capacitor, and decoupling transformer were mounted securely to the test probe and wired in series. The probe was then anchored into its lead shield bucket. As described in Section 3.3, the secondary of the isolation transformer was accessible through a connector on the top plate of the probe. The configuration of this probe and its associated instrumentation is shown in Fig. 4.3. This instrumentation is quite simple: a 9 V battery with switch and an oscilloscope are wired to the top plate connector.

Each of the two test inductors was measured in an identical manner. After installing and precooling the probe with liquid nitrogen, we began transferring liquid helium until the transformer became superconducting. Since the other critical components were mounted below the transformer, this cooling was assumed to be sufficient. The scope was set to a horizontal sweep speed of 0.2 cm/sec and placed in the single trace, manually triggered mode. The switch in the battery was closed briefly, and when it was opened, the scope was triggered. The resulting display of the decaying envelope was photographed with the oscilloscope camera.

The photographs were taken using both 5 mV/cm and 20 mV/cm vertical sensitivities so we could verify that the decay rate was amplitude independent. By taking careful measurements from the photographs, we determined the time required for the envelope to decay by a factor of  $1/e$ . According to basic circuit theory, the  $Q$  of the L-C network is related to this time,  $\tau$ , by

$$Q = \omega_0 \tau / 2 \quad (4.3.1)$$

In Table 4.2 we present the results of our tests on the two inductors. Since no difference could be seen between the measurements performed at different amplitude, we have not included this information. The accuracy of the  $Q$  determination was about 10%.



ANTENNA NOISE TEST SETUP

FIG 4.3

Table 4.2 Resonant Circuit Characteristics

| Inductor Material | Resonant Frequency | Q Factor | Equivalent Resistance | Thermal Noise Voltage                            |
|-------------------|--------------------|----------|-----------------------|--|
| Solid Nb-Ti       | 3155 Hz            | 6400     | 0.072 $\Omega$        | $4.1 \times 10^{-12} \text{ V}/\sqrt{\text{Hz}}$ |
| Cu Clad Nb-Ti     | 3443 Hz            | 5900     | 0.071 $\Omega$        | $4.1 \times 10^{-12} \text{ V}/\sqrt{\text{Hz}}$ |

Since the resonating capacitor had a measured value of 0.11  $\mu\text{F}$  we can determine its reactance at resonance. With this information and the appropriate Q factor, the equivalent resistance and its 4.2 K noise voltage are easily found. Appendix A gives the appropriate equations.

Given an antenna geometry, this noise voltage can be written in terms of an equivalent magnetic field noise. This is done for the case of our full size antenna in Section 5.1

#### 4.4 Dissipation Due to Cryostat

We used the mock induction coil and fiberglass wrapping form described in Section 3.4. The electronic instrumentation comprised a P.A.R. Model 124 amplifier and a Data Precision Model 2540A1 digital voltmeter. The insulating material which we tested was designated as NRC-2 made by the King-Seeley Thermos Co., Winchester, Mass. This material consists of 0.00025" polyester film coated on one side with 250  $\text{\AA}$  of aluminum. The resistivity of the material, as received, is about 1.5 ohms/square.

For our initial test of the NRS-2, we wrapped 50 layers of it on the fiberglass form at a density of about 100 turns-per-inch. The bottom of the form was also insulated by folding wedge-shaped pieces of the insulation over the end interleaving them.

We resonated the mock induction coil with a 0.1  $\mu\text{F}$  capacitor and drove this circuit through a 500 K  $\Omega$  dropping resistor from the reference output of the P.A.R. 124 amplifier. We connected the signal channel input of the amplifier across the inductor coil to monitor the circuit voltage. This circuit resonated at 3350 Hz with a Q factor of 5.4. The P.A.R. amplifier was operated in its tuned amplifier mode, and the offset adjustment control was used to null the output voltage. This nulled voltage was monitored on the D.V.M.



Our procedure was to raise and lower the insulated fiberglass form over the mock induction coil and note the change in voltage across the resonant circuit. This voltage change divided by the offset voltage is the  $\Delta V/V$  factor of Eq. D.14. The as-received superinsulation had  $\Delta V/V = 0.087$ . If we make the conservative assumption that the effective average temperature of this superinsulation is 200 K, then we obtain a value of  $2.9 \times 10^{-10} \text{ V}/\sqrt{\text{Hz}}$  for the thermal noise voltage in the antenna.

This noise level was clearly too high, so we unwrapped the superinsulation and processed it to raise its surface resistivity. This technique is proprietary with S.H.E. Corporation and was developed prior to award of this contract.

The winding form was re-wrapped with this processed NRC-2 in our previously described manner. When this material was tested, we found that at 3350 Hz the  $\Delta V/V$  was  $(4 \pm 4) \times 10^{-5}$ . In order to do this measurement more accurately, we increased the resonant frequency of the tank to 10.5 kHz by substituting a 0.01  $\mu\text{F}$  capacitor for the 0.1  $\mu\text{F}$  capacitor. According to Eq. D.7 in Appendix D, the size of the  $\Delta V/V$  factor scales as  $\omega^2$ , so this method enabled us to improve our measurement substantially. We observed  $\Delta V/V = (7.5 \pm 1.3) \times 10^{-4}$  at this frequency, implying that the value at 3000 Hz would be  $6.1 \times 10^{-5}$ . Again, assuming a temperature of 200 K for the superinsulation we obtain an additional thermal noise voltage of  $7.5 \times 10^{-12} \text{ V}/\sqrt{\text{Hz}}$  in the resonant circuit.

Within the sensitivity of our technique ( $\Delta V/V < 1.0 \times 10^{-5}$  referred to 3000 Hz) we could see no dissipation when we measured the thermal shield described in Section 3.4.

#### 4.5 Noise of Model Receiver

We used a P.A.R. Model 124 amplifier and a Ballantine Model 5500A counter to make spot measurements of the model receiver noise level. The receiver was operated with both primary and secondary feedback connected. The input of the amplifier was connected, through a 104:1 voltage divider, to the receiver output of the amplifier's reference oscillator.

We operated the P.A.R. in its unlocked (tuned voltmeter) mode with the Q set at 100. The reference channel oscillator was set to the desired frequency by using the counter, then the signal channel was tuned to this reference channel output. This technique was used to accurately set the center frequency for each of our spot noise measurements.

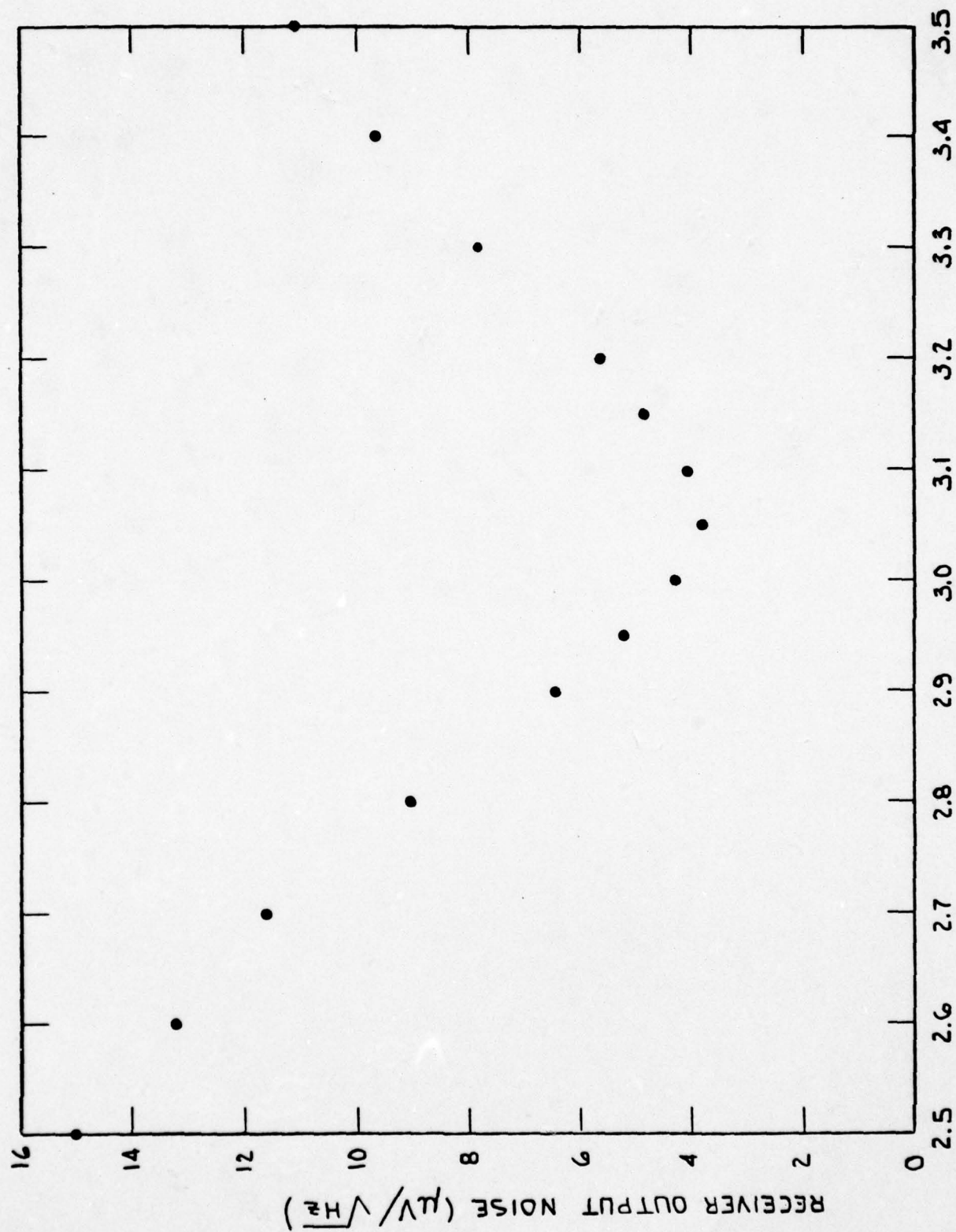
The noise was observed on the P.A.R.'s output meter after being rolled off by a two pole  $\tau = 10$  sec low pass filter. Our estimated error in these noise voltages is  $\pm 10\%$ . The meter reading was converted to a per-root-Hertz noise voltage referred to the receiver output. This was done by using an effective noise bandwidth of 1.23% and multiplying by 104 to account for the attenuator. P.A.R. specified this 1.23% effective noise bandwidth to be characteristic of the  $Q = 100$  filter position. The fact that it is not the expected 1.0% is due to the peak detecting nature of the instrument's signal rectifier.

The results of these noise measurements may be seen in Fig. 4.4. Note that the minimum lies 50 Hz above the natural resonant frequency of the antenna circuit. This shift is apparently due to the presence of the secondary feedback, although we have not verified the explanation by performing the required circuit analysis.

#### 4.6 Dynamic Range of Model Receiver

The dynamic range is defined as the ratio between the per-root-Hertz noise level and the maximum signal which can be received in the bandwidth of the instrument. Since in Section 4.5 we have measured the noise level, all that remains is to determine the largest output amplitude which can be obtained at 3000 Hz without excessive unlocking of the primary or secondary feedback loops.

For this measurement we used a Hewlett-Packard Model 200CD oscillator, a P.A.R. Model 124 amplifier, and a 104:1 attenuator network. The test signal from the oscillator was injected into the coupling loop of the model receiver through a 500 K $\Omega$  current limiting resistor, and the oscillator was set to 3000 Hz. Both the primary and secondary feedback paths were connected. The output of the receiver was connected to the P.A.R. amplifier through the attenuator. The amplifier was then placed in its unlocked mode (with a Q factor of 20) and was tuned for maximum response. The gain calibration of the amplifier was checked by substituting the instrument's calibration signal for the output of the model receiver.



NOISE VS. FREQUENCY FOR MODEL RECEIVER  
FIG 4.4



We found that at resonance the receiver was able to track a 6.3 V rms sine wave without "breaking lock" more often than once every 30 seconds. Even when this did occur the receiver was able to immediately reacquire the signal and resume tracking. Comparing this maximum amplitude with the noise levels obtained in Section 4.5, we find that the dynamic range at 3000 Hz is 124 dB. This drops to a worst case value of 122 dB for an operating bandwidth of 200 Hz.

#### 4.7 Linearity of Model Receiver

The instruments used in this measurement were two Hewlett-Packard Model 204 test oscillators, P.A.R. Model 124 amplifier and a Ballantine Model 5500A counter. In addition, we constructed three twin "T" notch filters, a harmonic generator network and two active tuned filters specially for this test.

The twin "T" filters were designed to reject 545 Hz, 1784 Hz, and 3530 Hz signals. The overall component matching for these filters was about 1%, but the notch frequency was separately trimmed to  $\pm 5$  Hz in each case. The harmonic generator was simply a diode network which could be switched to cause either a rectification or a symmetric clipping of the signal presented to it. These distortions primarily generated even or odd harmonics of the input frequency respectively. The 3 kHz bandpass amplifiers each used three type 741 operational amplifiers in the configuration of an infinite gain, state variable filter. The Q of these amplifiers was set to about 20. Each of these units was built into its own small metal box fitted with BNC connectors.

These instruments, networks, and filters were configured as shown in Fig. 4.5. The current which was driven in the coupling loop was quite accurately the algebraic sum of the two H.P. oscillator outputs. This current generated voltages in the induction coil which simulated the presence of large out-of-band magnetic fields at the model receiver input. The receiver was operated with both the primary and secondary feedback paths connected.

The receiver output was run through the twin "T" filters to remove the two large amplitude drive frequencies. The remaining signal was then taken through one of the bandpass filters to attenuate the remaining self harmonics of the two drive signals. Even though the H.P. oscillators were chosen for their low distortion (0.5%), these self harmonics were as much as 80 dB larger than the interharmonic

# RECEIVER UNDER TEST

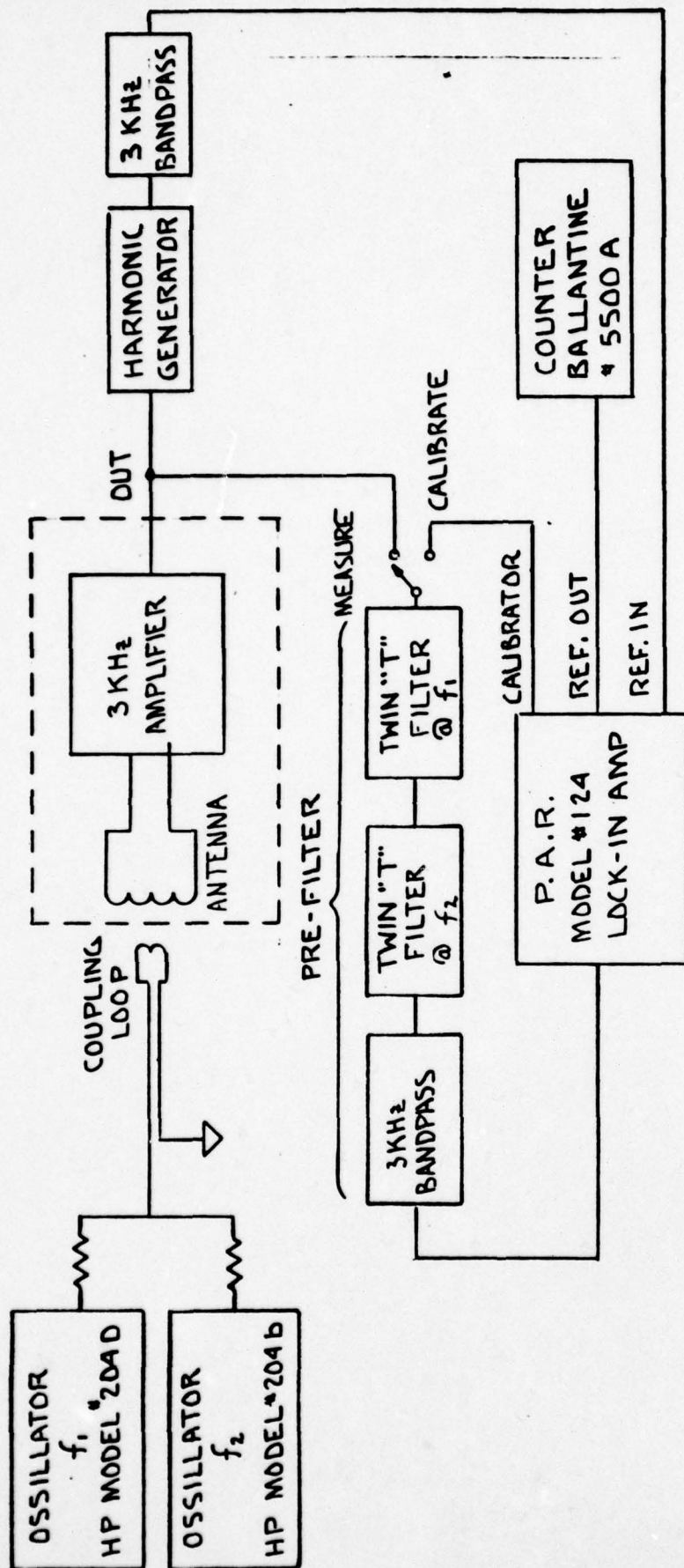


FIG 4.5

| SYMBOL |  | REVISION DESCRIPTION |  | BY | DATE | SCALE | SHEET 1 OF 1 |  | ASSY. DWG. | DWG. NO.   | REV. |
|--------|--|----------------------|--|----|------|-------|--------------|--|------------|------------|------|
|        |  |                      |  |    |      |       |              |  |            | A 2000-278 |      |
|        |  |                      |  |    |      |       |              |  |            |            |      |
|        |  |                      |  |    |      |       |              |  |            |            |      |
|        |  |                      |  |    |      |       |              |  |            |            |      |
|        |  |                      |  |    |      |       |              |  |            |            |      |
|        |  |                      |  |    |      |       |              |  |            |            |      |
|        |  |                      |  |    |      |       |              |  |            |            |      |
|        |  |                      |  |    |      |       |              |  |            |            |      |
|        |  |                      |  |    |      |       |              |  |            |            |      |
|        |  |                      |  |    |      |       |              |  |            |            |      |
|        |  |                      |  |    |      |       |              |  |            |            |      |
|        |  |                      |  |    |      |       |              |  |            |            |      |
|        |  |                      |  |    |      |       |              |  |            |            |      |
|        |  |                      |  |    |      |       |              |  |            |            |      |
|        |  |                      |  |    |      |       |              |  |            |            |      |
|        |  |                      |  |    |      |       |              |  |            |            |      |
|        |  |                      |  |    |      |       |              |  |            |            |      |
|        |  |                      |  |    |      |       |              |  |            |            |      |
|        |  |                      |  |    |      |       |              |  |            |            |      |
|        |  |                      |  |    |      |       |              |  |            |            |      |
|        |  |                      |  |    |      |       |              |  |            |            |      |
|        |  |                      |  |    |      |       |              |  |            |            |      |
|        |  |                      |  |    |      |       |              |  |            |            |      |
|        |  |                      |  |    |      |       |              |  |            |            |      |
|        |  |                      |  |    |      |       |              |  |            |            |      |
|        |  |                      |  |    |      |       |              |  |            |            |      |
|        |  |                      |  |    |      |       |              |  |            |            |      |
|        |  |                      |  |    |      |       |              |  |            |            |      |
|        |  |                      |  |    |      |       |              |  |            |            |      |
|        |  |                      |  |    |      |       |              |  |            |            |      |
|        |  |                      |  |    |      |       |              |  |            |            |      |
|        |  |                      |  |    |      |       |              |  |            |            |      |
|        |  |                      |  |    |      |       |              |  |            |            |      |
|        |  |                      |  |    |      |       |              |  |            |            |      |
|        |  |                      |  |    |      |       |              |  |            |            |      |
|        |  |                      |  |    |      |       |              |  |            |            |      |
|        |  |                      |  |    |      |       |              |  |            |            |      |
|        |  |                      |  |    |      |       |              |  |            |            |      |
|        |  |                      |  |    |      |       |              |  |            |            |      |
|        |  |                      |  |    |      |       |              |  |            |            |      |
|        |  |                      |  |    |      |       |              |  |            |            |      |
|        |  |                      |  |    |      |       |              |  |            |            |      |
|        |  |                      |  |    |      |       |              |  |            |            |      |
|        |  |                      |  |    |      |       |              |  |            |            |      |
|        |  |                      |  |    |      |       |              |  |            |            |      |
|        |  |                      |  |    |      |       |              |  |            |            |      |
|        |  |                      |  |    |      |       |              |  |            |            |      |
|        |  |                      |  |    |      |       |              |  |            |            |      |
|        |  |                      |  |    |      |       |              |  |            |            |      |
|        |  |                      |  |    |      |       |              |  |            |            |      |
|        |  |                      |  |    |      |       |              |  |            |            |      |
|        |  |                      |  |    |      |       |              |  |            |            |      |
|        |  |                      |  |    |      |       |              |  |            |            |      |
|        |  |                      |  |    |      |       |              |  |            |            |      |
|        |  |                      |  |    |      |       |              |  |            |            |      |
|        |  |                      |  |    |      |       |              |  |            |            |      |
|        |  |                      |  |    |      |       |              |  |            |            |      |
|        |  |                      |  |    |      |       |              |  |            |            |      |
|        |  |                      |  |    |      |       |              |  |            |            |      |
|        |  |                      |  |    |      |       |              |  |            |            |      |
|        |  |                      |  |    |      |       |              |  |            |            |      |
|        |  |                      |  |    |      |       |              |  |            |            |      |
|        |  |                      |  |    |      |       |              |  |            |            |      |
|        |  |                      |  |    |      |       |              |  |            |            |      |
|        |  |                      |  |    |      |       |              |  |            |            |      |
|        |  |                      |  |    |      |       |              |  |            |            |      |
|        |  |                      |  |    |      |       |              |  |            |            |      |
|        |  |                      |  |    |      |       |              |  |            |            |      |
|        |  |                      |  |    |      |       |              |  |            |            |      |
|        |  |                      |  |    |      |       |              |  |            |            |      |
|        |  |                      |  |    |      |       |              |  |            |            |      |
|        |  |                      |  |    |      |       |              |  |            |            |      |
|        |  |                      |  |    |      |       |              |  |            |            |      |
|        |  |                      |  |    |      |       |              |  |            |            |      |
|        |  |                      |  |    |      |       |              |  |            |            |      |
|        |  |                      |  |    |      |       |              |  |            |            |      |
|        |  |                      |  |    |      |       |              |  |            |            |      |
|        |  |                      |  |    |      |       |              |  |            |            |      |
|        |  |                      |  |    |      |       |              |  |            |            |      |
|        |  |                      |  |    |      |       |              |  |            |            |      |
|        |  |                      |  |    |      |       |              |  |            |            |      |
|        |  |                      |  |    |      |       |              |  |            |            |      |
|        |  |                      |  |    |      |       |              |  |            |            |      |
|        |  |                      |  |    |      |       |              |  |            |            |      |
|        |  |                      |  |    |      |       |              |  |            |            |      |
|        |  |                      |  |    |      |       |              |  |            |            |      |
|        |  |                      |  |    |      |       |              |  |            |            |      |
|        |  |                      |  |    |      |       |              |  |            |            |      |
|        |  |                      |  |    |      |       |              |  |            |            |      |
|        |  |                      |  |    |      |       |              |  |            |            |      |
|        |  |                      |  |    |      |       |              |  |            |            |      |
|        |  |                      |  |    |      |       |              |  |            |            |      |
|        |  |                      |  |    |      |       |              |  |            |            |      |
|        |  |                      |  |    |      |       |              |  |            |            |      |
|        |  |                      |  |    |      |       |              |  |            |            |      |
|        |  |                      |  |    |      |       |              |  |            |            |      |

signals of interest at 3 kHz. After this substantial pre-filtering, it was then possible to run the model receiver's output into the P.A.R. amplifier without overloading its input stages.

The harmonic generator was also connected to the output of the model receiver, and was set to the required symmetry. The tuned amplifier which followed this generator enabled us to select the desired 3 kHz mixing product from a complex background of other frequencies. This signal was sufficiently "clean" so that it could be used to phase lock the reference oscillator in the P.A.R. amplifier.

Our set-up procedure was to accurately adjust the frequencies of two H.P. oscillators to the notch frequencies of the twin "T" filters by using the Ballantine counter. We then calculated the specific frequency of the required intermodulation term. The oscillator outputs were set to the desired level, and we verified, again using the counter, that the P.A.R. reference channel was being phase locked to this calculated frequency. When properly locked the measured output frequency of the reference channel equaled the calculated frequency to within the  $\pm 1$  Hz resolution of the counter.

The operating frequency of the P.A.R. voltage calibrator is identical to that of the reference channel, so we could both tune and calibrate the signal channel of the instrument by connecting it to this output. In fact, by connecting the calibrator output to the input of the pre-filter we were able to conveniently include the net gain of these units in our amplitude calibration. The P.A.R. was operated at a Q of 20, in its wide dynamic range mode, and with a post detection bandwidth of 0.0125 Hz.

The two drive frequencies used for the test of even symmetry distortion were 545 Hz and 3530 Hz. We looked for their mixing signal at the difference frequency of 2985 Hz. For the test of odd symmetry distortion we drove the receiver at 545 Hz and 1784 Hz, and looked for a mixing signal at 3023 Hz ( $2 \times 1784 - 545$ ). We measured the distortion in each symmetry case for several oscillator amplitudes. Each oscillator was set to contribute equally to the amplitude of the receiver output.

The actual mixing signal was quite difficult to measure accurately or reproducibly. If there was measurable harmonic distortion we had expected to find a signal at the output of the P.A.R. detector which was stationary both in amplitude and phase.



The magnitude of this signal would then clearly be the rms value of the harmonic distortion. What we found, however, was that while the signal was usually much larger than the noise background per unit bandwidth, its amplitude and phase would change randomly over periods of a few seconds to a few tens of seconds.

Although the correctness of our approach is not entirely obvious, we have chosen to characterize this response as an intermodulation signal whose generating mechanism is fluctuating with time. We have visually estimated the average signal amplitude over a 60 second period for two settings of the reference phase  $90^\circ$  apart. These two averages were added in quadrature to get the total magnitude of the signal. This process was repeated several times for each of four different drive amplitudes. The results of these measurements for both the even and odd harmonic configurations are given in Table 4.3. To give an understanding of the reproducibility of these measurements, we have included the range of signal amplitudes seen at different times for each drive level.

Table 4.3 Interharmonic Distortion

| Drive Amplitude (Total) | Even Harmonic Amplitude (Min - Max) | Odd Harmonic Amplitude (Min - Max) |
|-------------------------|-------------------------------------|------------------------------------|
| 8 V p-p                 | 8 - 28 $\mu$ V                      | 5 - 13 $\mu$ V                     |
| 12                      | 270 - 306                           | 33 - 37                            |
| 16                      | 135 - 270                           | 8 - 27                             |
| 20                      | 45 - 109                            | 11 - 30                            |

In spite of the large scatter seen in this table we can at least make two observations. First, the receiver appeared to be much more susceptible to even symmetry harmonic generating processes. Second, the drive amplitudes which were most prone to cause large distortion were much smaller than the 20 V p-p output range of the receiver. These distortion amplitudes may be compared with the white noise level of approximately  $4 \mu\text{V}/\sqrt{\text{Hz}}$  in the receiver's passband.

## 5. CONCLUSIONS

### 5.1 Performance of a Full Scale Receiver

From the measurements we performed on the model receiver, on the test inductors, and on the cryostat materials, we can predict with some confidence the performance obtainable with an actual 3 kHz receiver system. However, in order to write the voltage gains and noise levels measured in these tests in terms of ambient magnetic fields, we must first specify the size of the induction coil or "antenna".

Following the arguments of Section 2.1 we have chosen, as our standard, a rectangular cross section coil 76 cm high  $\times$  17 cm wide  $\times$  17 cm long. This coil has a volume of  $2.2 \times 10^4 \text{ cm}^3$ , an area of  $1292 \text{ cm}^2$ , and a shape factor  $\lambda = 0.56$ . Using Eq. B.7 we can determine how many turns would be required on this antenna to equal the inductance of the induction coil of the model receiver. The result is that 199 turns would be needed to obtain 21.1 mH. Voltage induced in the antenna,  $V_I$ , is related to applied magnetic field,  $B_A$ , by

$$\frac{V_I}{B_A} = \omega N A \quad . \quad (5.1.1)$$

Near resonance, Eq. 3.7.1 relates the receiver's output voltage,  $V_o$ , to the induction coil voltage through the vector  $V_o/V_I = 3.6 \times 10^5$ . Therefore, at 3 kHz we would expect to obtain an overall system gain of

$$\frac{V_o}{B_A} = 1.75 \times 10^{11} \text{ Volts/Tesla} \quad . \quad (5.1.2)$$

We could re-label the ordinate of Fig. 4.1 in terms of  $V_o/B_A$  by scaling it to show this  $1.75 \times 10^{11} \text{ V/T}$  value at 3 kHz. The graph would then properly give the  $V_o/B_A$  gain versus frequency characteristics of the receiver.

Our model receiver could track 17.7 V pps signals at 3 kHz, implying that the full scale receiver could follow magnetic fields of  $1.0 \times 10^{-10} \text{ T p-p}$  at this frequency. Due to the tuned configuration of the input, however, the receiver can successfully track rather large fields at low frequencies. For example, at

## 5. CONCLUSIONS

### 5.1 Performance of a Full Scale Receiver

From the measurements we performed on the model receiver, on the test inductors, and on the cryostat materials, we can predict with some confidence the performance obtainable with an actual 3 kHz receiver system. However, in order to write the voltage gains and noise levels measured in these tests in terms of ambient magnetic fields, we must first specify the size of the induction coil or "antenna".

Following the arguments of Section 2.1 we have chosen, as our standard, a rectangular cross section coil 76 cm high  $\times$  17 cm wide  $\times$  17 cm long. This coil has a volume of  $2.2 \times 10^4 \text{ cm}^3$ , an area of  $1292 \text{ cm}^2$ , and a shape factor  $\lambda = 0.56$ . Using Eq. B.7 we can determine how many turns would be required on this antenna to equal the inductance of the induction coil of the model receiver. The result is that 199 turns would be needed to obtain 21.1 mH. Voltage induced in the antenna,  $V_I$ , is related to applied magnetic field,  $B_A$ , by

$$\frac{V_I}{B_A} = \omega N A \quad . \quad (5.1.1)$$

Near resonance, Eq. 3.7.1 relates the receiver's output voltage,  $V_O$ , to the induction coil voltage through the vector  $V_O/V_I = 3.6 \times 10^5$ . Therefore, at 3 kHz we would expect to obtain an overall system gain of

$$\frac{V_O}{B_A} = 1.75 \times 10^{11} \text{ Volts/Tesla} \quad . \quad (5.1.2)$$

We could re-label the ordinate of Fig. 4.1 in terms of  $V_O/B_A$  by scaling it to show this  $1.75 \times 10^{11} \text{ V/T}$  value at 3 kHz. The graph would then properly give the  $V_O/B_A$  gain versus frequency characteristics of the receiver.

Our model receiver could track 17.7 V pps signals at 3 kHz, implying that the full scale receiver could follow magnetic fields of  $1.0 \times 10^{-10} \text{ T p-p}$  at this frequency. Due to the tuned configuration of the input, however, the receiver can successfully track rather large fields at low frequencies. For example, at



100 Hz, the receiver could follow at  $5.0 \times 10^{-8}$  T p-p magnetic disturbance. This range continues to improve at 6 dB per octave down to dc.

The noise data in Fig. 4.3 may be converted from  $V/\sqrt{\text{Hz}}$  to  $T/\sqrt{\text{Hz}}$  by use of Eq. 5.1.2. We find that  $f_o = 3050$  Hz the predicted noise level of our full scale receiver would be  $2.1 \times 10^{-17}$  T/ $\sqrt{\text{Hz}}$ . At  $f_o \pm 50$  Hz this degrades to  $2.4 \times 10^{-17}$  T/ $\sqrt{\text{Hz}}$  and at  $f_o \pm 100$  Hz the noise is  $2.9 \times 10^{-17}$  T/ $\sqrt{\text{Hz}}$ .

The effective noise in these bandwidths would be lower than this worst case figure at the band edge, and would depend on the distribution of "information density" throughout the band.

In Section 4.3 we measured the Q factors for superconducting resonant circuits at 3 kHz. The toroidal inductors used in these tests were large enough to roughly simulate the performance expected from the induction coil of a full scale receiver. Their thermal noise voltage was determined to be  $4.1 \times 10^{-12}$  V/ $\sqrt{\text{Hz}}$ . We can refer this voltage to the receiver output if we multiply  $V_o/V_i = 3.6 \times 10^5$ . Finally, we convert to equivalent magnetic field by applying Eq. 5.1.2. The result is that the intrinsic thermal noise of the antenna circuit should only be  $8.4 \times 10^{-18}$  T/ $\sqrt{\text{Hz}}$ .

Contributions to the noise from the cryostat were measured in Section 4.4. Superinsulation was the only material which was found to contribute measurably, but by "processing" the NRC-2 material we were able to reduce its contributions significantly. Assuming a rather pessimistic value of 200 K for the effective average temperature of superinsulation we found that a tightly fitting cryostat could be made which would contribute  $7.5 \times 10^{-12}$  V/ $\sqrt{\text{Hz}}$ . Following the logic of the preceding paragraph, this noise contribution amounts to  $1.5 \times 10^{-17}$  T/ $\sqrt{\text{Hz}}$  of additional uncorrelated noise in our full scale receiver.

The dynamic range of the model receiver was measured, in Section 4.6, to be 124 dB at 3050 Hz, referred to a unit bandwidth. This figure should also be nominally correct for the full scale receiver.

The linearity measurement in Section 4.7 was somewhat of a disappointment in terms of the Naval Research Lab's target specifications. They had hoped to see less than  $2 \times 10^{-17}$  T rms mixing products from large out-of-band signals.

Our worst case result was  $1.7 \times 10^{-15}$  T rms for even harmonic mixing. This figure seems surprisingly high and bears further investigation; however, the target specification may also be unnecessarily strict. Having a worst case mixing product equal in rms amplitude to the integrated noise in the receiver's bandwidth would appear to be an acceptable situation. For a 200 Hz bandwidth this would be  $2.8 \times 10^{-16}$  T.

## 5.2 Possibilities for Receiver Improvement

The receiver noise level is presently limited by three factors: 1) antenna gain, 2) energy matching between antenna and SQUID, and 3) SQUID energy sensitivity. The antenna's gain depends on its volume and the receiver's bandwidth, as discussed in Section 2.1. However, both of these characteristics may be predetermined by design constraints on the receiver system.

In our model receiver design we chose to couple only 10% of the antenna energy into the SQUID. In theory, this figure could be increased to 50%, giving a factor of 2.2 improvement in noise level. It is not known whether such tight coupling would cause qualitatively different behavior of the system, but this could be investigated rather easily.

Finally, the  $2.5 \times 10^{-29}$  J/Hz energy sensitivity of the SQUID could probably be improved by almost a factor of 2 through the use of a custom designed VHF amplifier having a 1.0 dB noise figure at 150 MHz. Our present Anzac amplifiers were designed to operate over a wide bandwidth with a low V.S.W.R. One should be able to obtain significant improvements in noise figure over a restricted bandwidth of a few MHz with some additional effort.

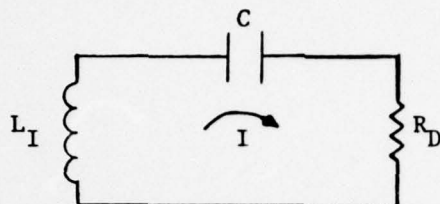
The nonlinearities seen by our measurement of interharmonic distortion may have possibly been due to signal correlated flux motion in the induction coil. This induction coil was a tightly wound, thick solenoid in the model receiver, so that a large fraction of its volume was occupied by its own superconducting wire. Furthermore, because of its small size, the magnetic field levels were about 100 times larger than would be present in a full scale induction coil, causing an increased driving force for moving trapped flux lines. The 545 Hz test signal which was applied to the induction coil in our tests generated peak fields

of about  $10^{-7}$  T, possibly enough to cause minute flux motion. This hypothesis could be checked by repeating the linearity measurements on the receiver probe when it had been cooled in a low magnetic field. If this were indeed the cause of the effect, it should disappear for the case of a full scale induction coil.



## APPENDIX A. ANTENNA NOISE

The induction coil  $L_I$  in this case is resonated with a series capacitor  $C$  and resistance  $R_D$  represents losses in both the pickup loop and the capacitor.



A magnetic field  $B_o$  at frequency  $\omega$  applied to the pickup loop induces a voltage in the loop given by (rms values are used throughout)

$$V = d\phi/dt = \omega N B_o A \quad (A.1)$$

where  $\phi$  is the total flux intercepted by the loop,  $A$  the loop area, and  $N$  the number of its turns. The rms noise voltage generated in bandwidth  $\delta f$  by the resistor  $R_D$  at temperature  $T_F$  is given by

$$V_n = \sqrt{4 k_B T_F R_D \delta f} \quad (A.2)$$

Thus the equivalent magnetic field noise  $B_n$  of the antenna due to  $R_D$  can be found by substituting Eq. A.2 into Eq. A.1 with the result that

$$\omega N B_n A = \sqrt{4 k_B T_F R_D \delta f} \quad (A.3)$$

where  $T_F$  is the temperature of the antenna and  $\delta f$  is the effective noise bandwidth. Taking  $\delta f = 1$  Hz, we have for the effective rms field noise per root Hz

$$B_n / \sqrt{\text{Hz}} = \left( \frac{4 k_B T_F L_I}{\omega Q N^2 A^2} \right)^{1/2} \quad (A.4)$$

In Eq. (A.4) we have introduced the flux transformer quality factor

$$Q = \omega L_I / R_D \quad (A.5)$$

The loop inductance may be written in terms of its size and shape factors as

$$L_I = \mu_o N^2 \lambda A / \ell \quad (A.6)$$

where  $\ell$  is the length of the loop and  $\lambda$ , a geometrical correction factor akin to Nagaoka's constant for a finite length coil, is a function of coil height,

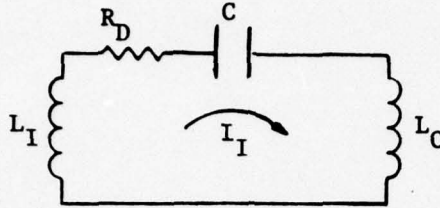
width and length. In general  $\lambda$  lies between zero and one, but for the "short" coils encountered in these flux transformers it is about 0.5. Using Eq. (A.6) we may finally write

$$B_n / \sqrt{\text{Hz}} = \left( \frac{4 k_B T_F \mu_0 \lambda}{\omega Q A \ell} \right)^{1/2} . \quad (\text{A.7})$$

Eq. (A.7) is also valid in the case of a nonresonant totally superconducting flux transformer, if we formally define  $Q$  by Eq. (A.5), where  $R_D$  now accounts only for the ac losses in the superconductor.

## APPENDIX B. ANTENNA ENERGY GAIN

We shall take for the resonant antenna input the following circuit:



The induction coil inductance is  $L_I$ , the total dissipation is represented by  $R_D$ , the resonating capacitor is  $C$  and  $L_C$  represents the apparent inductance of the following SQUID amplifier, i.e. the coupling inductance.

A magnetic field of amplitude  $B_o$  and frequency  $\omega$  is applied to the pickup coil and induces a voltage

$$V = \omega N B_o A \quad (B.1)$$

where  $N$  is the number of turns in the loop and  $A$  is its area. The equation for  $I_I$ , the current flowing in the tuned antenna coil, is

$$j\omega(L_I + L_C)I_I + I_I/j\omega C + R_D I_I - \omega N B_o A = 0 \quad (B.2)$$

which can be solved for  $I_I$  to give

$$I_I = \frac{N B_o A}{(L_I + L_C) \left[ \frac{1}{Q} + j \left( 1 - \frac{\omega_o^2}{\omega^2} \right) \right]}, \quad \omega_o^2 \equiv [(L_I + L_C)C]^{-1} \quad (B.3)$$

The circulating current is a maximum at  $\omega = \omega_o$  and drops as  $\omega$  approaches the upper or lower specified bandlimits,  $\omega = \omega_o \pm \Delta\omega$ . For our expected operating conditions ( $Q \geq 10^3$ ,  $\Delta\omega/2\pi = 100$  Hz,  $\omega/2\pi = 3$  kHz) we have

$$\frac{1}{Q} \ll \frac{2\Delta\omega}{\omega} \quad (B.4)$$

The significance of this inequality is that we are far enough from resonance at the bandlimits that we may drop the  $1/Q$  term in Eq. (B.3).



We will calculate the antenna current gain for this "worst case" condition at the bandlimits where  $\omega = \omega_0 \pm \Delta\omega$ .

Since  $\Delta\omega/\omega_0 \ll 1$ , we may make the approximation that

$$\left[ 1 - \frac{\omega_0^2}{(\omega_0 \pm \Delta\omega)^2} \right] \approx \pm 2\Delta\omega/\omega_0 \quad (B.5)$$

The expression for loop current then becomes

$$I_I = \frac{B_0 NA}{(L_I + L_C)(2\Delta\omega/\omega_0)} \quad (B.6)$$

It is important to note that the factor NA in the numerator of Eq. B.6 is related to  $L_I$  by

$$L_I = \mu_0 N^2 \lambda A / \ell \quad (B.7)$$

Here  $\mu_0$  is the permeability of free space,  $\ell$  is the length of the pickup coil and  $\lambda$  is a shape factor of order unity.

Let us define a factor  $\gamma = L_C/L_I$  which describes the relative amount of amplifier inductance coupled into this resonant circuit. We then have the following expression for current sensitivity

$$\frac{I_I}{B_0} = \frac{\omega NA}{L_I 2\Delta\omega (1 + \gamma)} \quad (B.8)$$

Energy sensitivity is a more fundamental concept for characterizing the antenna circuit, and can be derived using B.6 and B.7. We define the total energy as  $E_T \equiv \frac{1}{2}(L_I + L_C)I_I^2$ . Therefore,

$$\frac{E_T}{B_0^2} = \frac{A\ell}{2\mu_0 \lambda} \left( \frac{\omega}{2\Delta\omega} \right)^2 \frac{1}{(1 + \gamma)} \quad (B.9)$$

The most important energy is that which can be coupled to the SQUID amplifier, and is represented by  $E_C \equiv \frac{1}{2} L_C I_I^2$ .

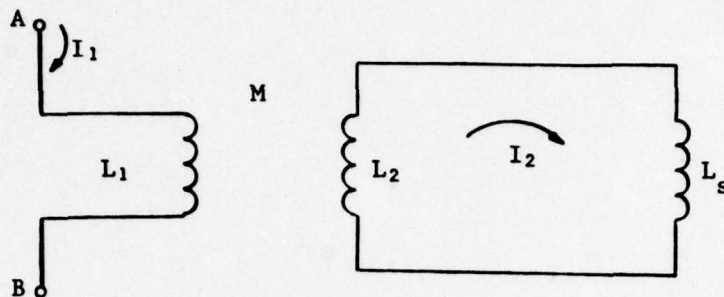
So that

$$\frac{E_C}{B_o^2} = \left( \frac{A\lambda}{2\mu_o \lambda} \right) \left( \frac{\omega}{2\Delta\omega} \right)^2 \frac{\gamma}{(1 + \gamma)^2} \quad (B.10)$$

This last equation can be taken as the available energy sensitivity for our induction antenna. The first factor describes its effective volume, the second is the gain due to resonating the circuit, and the third factor defines the behavior of the coupling inductance. This last factor has a maximum at  $\gamma = 1$ , which implies that, with the optimum matching,  $L_C = L_I$ , half of the total energy is available to the SQUID.

## APPENDIX C. MATCHING TRANSFORMER

For the circuit shown below we wish to calculate the effective input inductance  $L_c$  between points A and B and the current gain  $G \equiv I_2/I_1$ .



If the input is to look like an inductance  $L_c$ , then we must set

$$j\omega L_c I_1 \equiv j\omega L_1 I_1 - j\omega M I_2 \quad . \quad (C.1)$$

The equation for the secondary circuit is simply

$$j\omega L_2 I_2 + j\omega L_s I_2 - j\omega M I_1 = 0 \quad . \quad (C.2)$$

Combining these equations gives the two useful relationships

$$L_c = L_1 - \frac{M^2}{L_2 + L_s} \quad (C.3)$$

$$R \equiv I_2/I_1 = \frac{M}{L_2 + L_s} \quad . \quad (C.4)$$

Now let us define several quantities:

$$\text{Coupling Coefficient} \quad K \equiv M/(L_1 L_2)^{1/2} \quad (C.5)$$

$$\text{Transformation Ratio} \quad \eta \equiv L_1/L_2 \quad (C.6)$$

$$\text{Size Ratio} \quad \beta \equiv L_2/L_s \quad . \quad (C.7)$$

After some manipulation one finds that,

$$L_c = \eta L_s \left( \frac{\beta}{\beta + 1} \right) \left[ 1 + \beta (1 - K^2) \right] \quad (C.8)$$



and

$$R = \eta^{\frac{1}{2}} K \left( \frac{\beta}{1 + \beta} \right) . \quad (C.9)$$

In the limit of the ideal transformer ( $K = 1$  and  $\beta \rightarrow \infty$ ) Eq. C.8 and C.9 clearly reduce to the expected result.

If this limit does not obtain, we may optimize the circuit by maximizing  $R$  with respect to  $\beta$  by using C.8 to eliminate  $\eta$ . We must maximize

$$R = \left( \frac{L_c}{L_s} \right)^{\frac{1}{2}} K \left\{ \frac{\beta}{(1 + \beta)[1 + \beta(1 - K^2)]} \right\}^{\frac{1}{2}} . \quad (C.10)$$

The result is that the optimum size of the transformer is

$$\beta_{\text{opt}} \equiv \frac{L_2}{L_s} = (1 - K^2)^{-\frac{1}{2}} \quad (C.11)$$

And the optimum transformation ratio reduces to

$$\eta_{\text{opt}} = \left( \frac{L_c}{L_s} \right) \quad (C.12)$$

Then the current gain for this optimum but not ideal transformer is

$$R = \left( \frac{I_2}{I_1} \right) = \left( \frac{L_c}{L_s} \right)^{\frac{1}{2}} \frac{K}{1 + (1 - K^2)^{\frac{1}{2}}} . \quad (C.13)$$

If the transformer had been ideal we would have found that

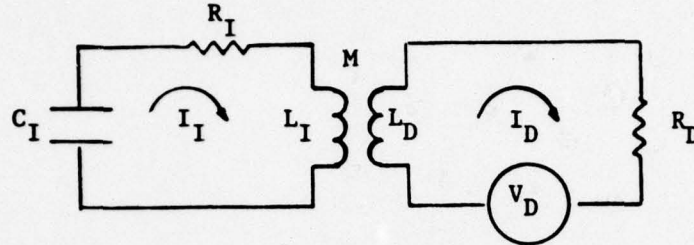
$$\frac{1}{2} L_c I_1^2 = \frac{1}{2} L_s I_2^2 . \quad (C.14)$$

The energy sensitivity of the SQUID is not degraded by an ideal transformer: its impedance is merely transformed. However, we can show immediately from Eq. C.13 that for a non-ideal transformer the energy sensitivity is reduced by the factor

$$\alpha = \frac{K^2}{\left[ 1 + (1 - K^2)^{\frac{1}{2}} \right]^2} \quad (C.15)$$

# APPENDIX D. NOISE CONTRIBUTIONS FROM CRYOSTAT

The circuit below shows the model we are assuming for the interaction between tank and dewar.



The tank circuit comprising  $C_I$  and  $L_I$  resonates at  $\omega_o$ . Internal dissipation  $R_I$  limits the natural quality factor to  $Q_o = \omega_o L_I / R_I$ . Dissipative material in the dewar is characterized by  $R_D$  and  $L_D$ . The thermal noise voltage  $V_D / \sqrt{\text{Hz}}$  in the dewar is given by

$$V_D / \sqrt{\text{Hz}} = (4 k_B T_D R_D)^{1/2}, \quad (\text{D.1})$$

and the mutual inductance is  $M$ .

The loop equations can be written as

$$\left( \frac{1}{j\omega C_I} + j\omega L_I + R_I \right) I_I - j\omega M I_D = 0 \quad (\text{D.2})$$

and,

$$(j\omega L_D + R_D) I_D - j\omega M I_I = V_D. \quad (\text{D.3})$$

Combining these equations to eliminate  $I_D$  gives

$$\left( \frac{1}{j\omega C_I} + j\omega L_I + R_I + \frac{\omega^2 M^2}{j\omega L_D + R_D} \right) I_I = \frac{j\omega M V_D}{j\omega L_D + R_D}. \quad (\text{D.4})$$

We now make the very reasonable assumption that the time constant of the dewar ( $L_D / R_D$ ) is much shorter than  $1/\omega_o$ . If this were not true, the presence of the

dewar would dramatically alter the resonant frequency of the tank circuit. Such an effect is not observed. The result is

$$\left[ \frac{1}{j\omega C_I} + j\omega L_I + \left( R_I + \frac{\omega^2 M^2}{R_D} \right) \right] I_I = \frac{j\omega M V_D}{R_D} \quad (D.5)$$

If we now introduce an equivalent voltage  $V_{eq}$  and an equivalent resistance  $R_{eq}$  defined by

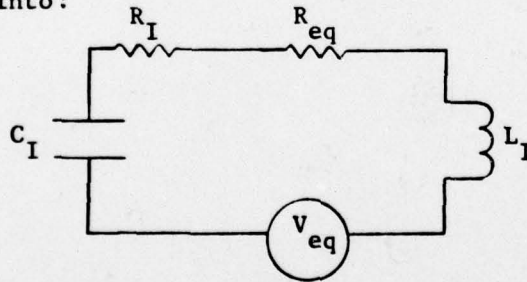
$$V_{eq} \equiv j\omega M V_D / R_D \quad (D.6)$$

$$R_{eq} \equiv \omega^2 M^2 / R_D \quad (D.7)$$

we may write Eq. D.5 in the form

$$\left( \frac{1}{j\omega C_I} + j\omega L_I + R_I + R_{eq} \right) I_I = V_{eq} \quad (D.8)$$

The equivalent circuit describing the dewar-tank circuit interaction has thus been transformed into:



Substitution of Eq. D.1 into Eq. D.6 yields an equation for the noise voltage  $V_n$  appearing in the tank due to the presence of the dewar

$$V_n / \sqrt{\text{Hz}} \equiv V_{eq} / \sqrt{\text{Hz}} \equiv \frac{\omega M}{R_D} (4 k_B T_D R_D)^{1/2} \quad (D.9)$$



Using Eq. D.7 to relate  $R_D$  to  $R_{eq}$ , we may also write Eq. D.9 in terms of  $R_{eq}$  as

$$V_n / \sqrt{\text{Hz}} = (4k_B T_D R_{eq})^{1/2} \quad (D.10)$$

Note that  $R_{eq}$  may be determined experimentally by measuring the change in the  $Q$  of the tank circuit when the tank is placed inside the dewar since, for small changes in  $Q$ ,

$$\Delta Q \equiv Q_o - Q = \frac{\omega_o L_I}{R_I} - \frac{\omega_o L_I}{R_I + R_{eq}} \approx Q_o \left( \frac{R_{eq}}{R_I} \right) \quad (D.11)$$

or

$$R_{eq} = \frac{\Delta Q}{Q_o} R_I \quad (D.12)$$

For a current source excitation of the tank at resonance, the peak voltage across  $L_I$  is proportional to  $Q$ , so we may also determine  $R_{eq}$  from

$$R_{eq} = \frac{\Delta V}{V} R_I \quad (D.13)$$

Combination of Eq. D.10 and Eq. D.13 produces the final result

$$V_n / \sqrt{\text{Hz}} = \left[ 4 k_B T_D R_I (\Delta V/V) \right]^{1/2} \quad (D.14)$$

Thus we see that by estimating  $T_D$  and by measuring the change in voltage across  $L_I$  as the tank is placed inside the dewar, we can easily determine the noise generated in the tank circuit at resonance due to external dissipative materials. No information about  $L_D$ ,  $M$ , or  $R_D$  is required.